PRODUCTION AND CHARACTERIZATION OF WATER SOLUBLE CdSeTe BASED CORE/SHELL NANOCRYSTALS AND THEIR APPLICATIONS IN BIOIMAGING

A Thesis Submitted to
the Graduate School of Engineering and Science of
İzmir Institute of Technology
in Partial Fulfillment of the Requirements for the Degree of

MASTER OF SCIENCE

in Chemistry

by
Seda ÖZDEMİR

July 2009
İZMİR

We approve the thesis of **Seda ÖZDEMİR**

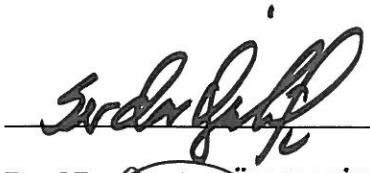

Prof.Dr. Serdar ÖZÇELİK
Supervisor

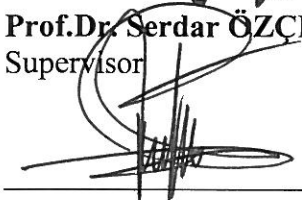

Assoc.Prof.Dr. Mustafa Muammer DEMİR
Committee Member

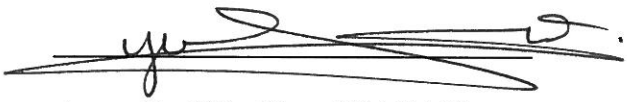

Assoc.Prof.Dr. Yusuf BARAN
Committee Member

3 July 2009

Date

Prof.Dr. Levent ARTOK
Head of the Chemistry Department

Prof.Dr. Hasan BÖKE
Dean of the Graduate School of
Engineering and Sciences

ACKNOWLEDGEMENTS

First, I would like to express my appreciation to my master's thesis advisor, Prof. Dr. Serdar ÖZÇELİK, who believed me at the beginning of this academic program. During this thesis study he always encouraged me and helped me with his valuable advices.

Also, I would like to thank Assist. Prof. Mahmut KUŞ, Caner ÜNLÜ, Leyla DOĞAN and Gülay DURGUN for their constructive comments and supports on this study.

Additionally, I would like to acknowledge my colleagues Çiçek KARŞAL, Figen GAZİOĞLU, Zeynep KAYA, Ferit ÖZAY, Oya ŞAHİN for their wonderful and enjoyable friendship. Special thanks to all my friends in IYTE Chemistry Department, especially Özlem KEPENEKÇİ, Pınar KASAPLAR and Nesrin HORZUM.

I want to thank Specialist Özgür YILMAZER, Ph.D student Murat ÇOKAKLI and İYTE-MAM specialist for their helps during my thesis studies.

Finally, I would like to express my thanks to my lovely family, my father Ziya, my mother Birgül, my sister Seçil and my cousin Ece for their love, understanding, motivation and continuous support.

ABSTRACT

PRODUCTION AND CHARACTERIZATION OF WATER SOLUBLE CdSeTe BASED CORE/SHELL NANOCRYSTALS AND THEIR APPLICATIONS IN BIOIMAGING

In recent years, nanotechnology has become one of the most intensively studied fields. At the nanometer scale, materials have unique electrical, optical, magnetic and chemical properties. They can be used for a wide variety of applications such as electro-optical devices, tagging and medical applications. The goal of this study was to produce water-dispersible alloyed $CdSe_xTe_{1-x}$ semiconductor nanocrystals, which are suitable to interact with biomolecules. $CdSe_xTe_{1-x}$ nanocrystals were synthesized by a single step aqueous synthesis method. Monodisperse, $CdSe_xTe_{1-x}$ nanocrystals with zinc blende structure were obtained in water. Synthesized nanocrystals emit in the range from 528 nm to 620 nm. $CdSe_xTe_{1-x}$ nanocrystals have 17% photoluminescence quantum yield, after the CdS shell coating the photoluminescence quantum yield increased up to 22%. MTT test and Trypan Blue tests were used to evaluate the toxicity of $CdSe_xTe_{1-x}$ nanocrystals. MTT measurements reveal that the MCF7 cancer cells are not affected by the nanocrystals at any dosage and exposure condition, but lethal effects are determined at the concentration of 1.0μg/ml for the PC3 cells. The BEAS 2B cells are very sensitive to the nanocrystals and do not proliferate at concentration of 0.5μg/ml. Confocal microscopy studies show that the nanocrystals has ability to penetrate to the cytoplasm of cells.

ÖZET

SUDA ÇÖZÜLEBİLEN CdSeTe TABANLI ÇEKİRDEK/KABUK NANOKRİSTALLERİNİN ÜRETİLMESİ, KARAKTERİZASYONU VE BİYOGÖRÜNTÜLEME UYGULAMALARI

Nanoteknoloji, son yıllarda, en kapsamlı çalışmaların yapıldığı alanlardan biri haline geldi. Nanometre mertebesinde, malzemeler benzersiz elektiriksel, optik, manyetik ve kimyasal özelliklere sahiptirler. Eşsiz özellikleri sayesinde bu malzemeler elektro-optik aygıtlar, işaretleme ve tıbbi uygulamalar gibi geniş kapsamlı uygulama alanlarına sahiptirler. Bu çalışmanın hedefi, biyomoleküller ile etkileşmeye uygun, suda çözünebilen $CdSe_xTe_{1-x}$ alaşım yarı iletken nanokristaller elde etmektir. $CdSe_xTe_{1-x}$ yarı iletken nanokristaller tek basamakta sentez yöntemi ile elde edilmişlerdir. Eş büyüklükte, çinko karışım yapılı $CdSe_xTe_{1-x}$ nanokristaller su içinde çözünmüş olarak hazırlanmışlardır. Sentezlenen nanokristaller 528nm den 620nm ye kadar geniş aralıkta ışıma yapmaktadırlar. Alaşım $CdSe_xTe_{1-x}$ nanokristallerin fotoluminesans kuantum verimi 17% iken, CdS kabuğu ile kaplandıktan sonra fotoluminesans kuantum verimi 22% ye yükselmiştir. $CdSe_xTe_{1-x}$ nanokristallerin toksisitelerinin belirlenmesinde MTT ve Trypan mavisi testleri kullanılmıştır. MTT sonuçları MCF7 hücrelerinin hiçbir doz ve konsantrasyonda nanokristallerden etkilenmediğini fakat PC3 hücrelerinde 1.0µg/ml konsantrasyonda ölümcül etkilerin başladığını ortaya koymaktadır. BEAS 2B hücrelerinin nanokristallere çok hassas olduğu ve 0.5µg/ml konsantrasyonda hücre çoğalmasının durduğu belirlenmiştir. Nanokristallerin hücre sitoplazmasına geçtme yetisinde oldukları, konfokal mikroskopi çalışmaları ile belirlenmiştir.

TABLE OF CONTENTS

LIST OF FIGURES

LIST OF TABLES

CHAPTER 1

INTRODUCTION

1.1. The Purpose of the Study

The purpose of the study is to synthesize and characterize water dispersible CdSeTe based core/shell nanocrystals by tuning spectral properties, varying their size. The nanocrystals are aimed to be used in bioimaging applications, as such confocal microscopy.

1.2. Quantum Dots and Biotechnology

Developments of nanocrystal technology start in the early 1980s by two research groups, Alexander Efros and Alexie Ekimov were at the Yoffe Institute, Russia, and Louis Brus and his team was at Bell Laboratories. Two of the Bell Labs investigators, Moungi Bawendi and Paul Alivisatos, made the nanoparticles water-dispersible and devised inorganic shells to enhance their fluorescence (Edwards 2006).

Semiconductor quantum dots (QDs) are nanocrystalline materials, mostly composed of periodic groups of II-VI or III-V elements. These light emitting particles with diameters of 1-10nm show quantum confinement behavior, as the semiconductor's size becomes smaller, the band gap becomes larger. Size of the particle determines the electronic and physical properties of the material.

When the size of crystal is reduced, the surface area / volume ratio increases and surface structure affects optical and electronic properties strongly. Furthermore, the crystal's electronic properties stop behaving as bulk structure. This behavior is a result of quantum confinement effects, the behavior of electrons in a particle due to spatial restrictions.

Quantum dot fluorescence involves exciting an electron from the valence band of the semiconductor material across an energy gap, making it a conduction electron and leaving behind a hole. When the excited electron in the conduction band loses its excess energy, it returns to valance band and remerges with the hole. Light forms due to combination of electron and hole pair.

The electron-hole pair, which is known as exciton, is quantum confined by the small size of the nanocrystals. When the electron–hole pair eventually recombines, a characteristic photon is emitted. The confined nanocrystals grow with time and with this growing the energy band gap changes, thus the color of the fluorescence photon changes depending on the band gap energy, as illustrated by the schematic in Figure 1.1. The larger the band gap energy for a given material, the shorter the wavelength of the emitted photon (Deerinck, et al. 2008).

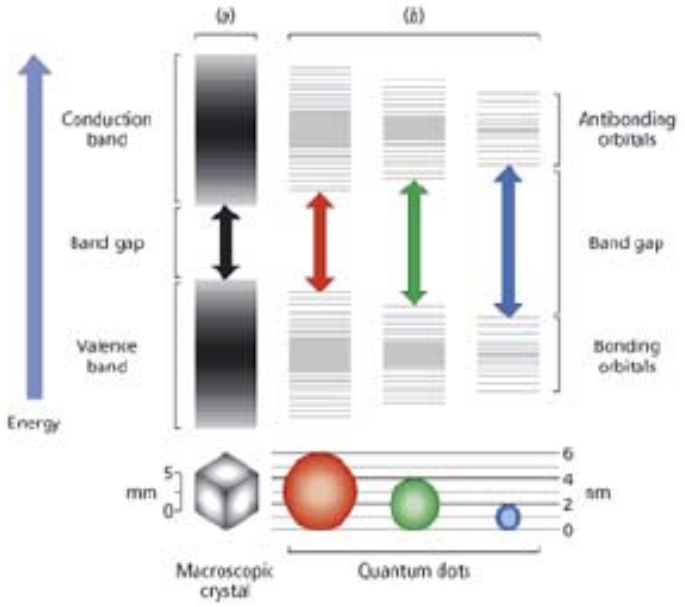

Figure 1.1. Schematic representation of band offsets of quantum dots.
(Source: www.evidenttech.com)

Due to the superior optical properties of QDs, they have potential applications in electronic devices such as memory devices and in optical devices such as light emitting systems such as LEDs and Lasers. Since Nie et al. and Alivisatos et al. published the first reports describing the use of QDs as fluorescent labels for biomolecules in 1998, QDs began to biocompatible and are suitable for using in biological and biomedical

applications, e.g. cell imaging (Bhatia, et al. 2004), detection and targeting of specific cells (Wu, et al. 2002) and labeling tissues (Akerman, et al. 2002).

QDs have broad absorption spectra, narrow and symmetric emission spectra (full width at half maximum ~40 nm), Figure 1.2. Long fluorescence lifetimes (hundreds of nanoseconds), high and stable quantum yield (the ratio of emitted to absorbed photons), and a large saturation intensity make them much brighter than fluorescence dyes (Pinaud, et al. 2006). Fluorescence dyes are limited by their narrow excitation range, low emission intensity and short lifetime.

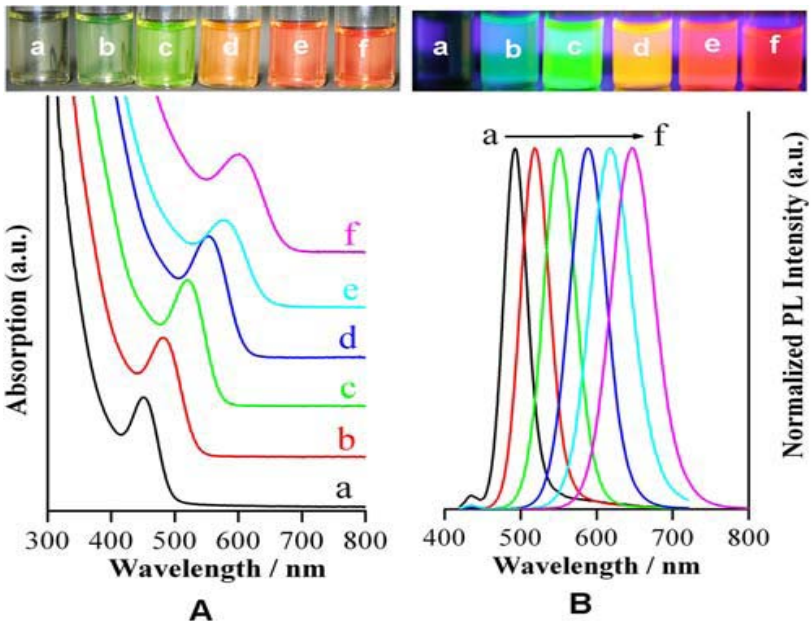

Figure 1.2. a) MSA-coated CdTe QDs under ambient conditions (top) and the absorption spectra (bottom); b) MSA-coated CdTe QDs under an UV lamp (top) and the photoluminescence spectra (bottom). (The photoluminescence were at a) 493 nm, b) 519 nm, c) 551 nm, d) 589 nm, e) 617 nm, f) 647 nm) (Source: Dong, et al. 2008)

1.3. Types of Quantum Dots

QDs have been synthesized using both two element systems (binary dots) and three-element systems (ternary alloy dots). Typical QDs are in core-shell structure (for example, CdSe core with a ZnS shell) or core-only (for example, CdTe) or alloyed (for example, $CdSe_xTe_{1-x}$) structures functionalized with different coatings. A core type quantum dot consists of two or three atoms. A core/shell quantum dot where the core surrounded with a shell, consisting of different kinds of atoms, show a great

enhancement in optical properties, such as quantum yield and photostability, and inherent toxicity of individual ions (Cd^{2+}, Se^{2-} and Te^{2-}).

Many research groups have tried to synthesize QDs with a core or a core/shell structures, such as CdSe, CdTe, CdS, ZnSe, CdHgTe, $CdSe_xS_{1-x}$ PbSe, InP, CdSe/CdS, CdSe/ZnS, CdS/ZnS, CdTe/ZnS, CdTe/CdS, $CdSe_{1-x}Te_x/CdS$. Mainly core/shell structures have been focused. Passivation of the nanocrystals surface by a thin semiconductor shell do not significantly change the absorption and emission wavelengths, but increases the quantum yield, as illustrated in Figure 1.3.

A controlled coating with proper shell conserves the charge carriers inside nanocrystals due to reducing the trap states, and improves photo-stability. This improvement is also due to the reduction of crystalline defects on the core surface by lattice matching of the two materials structure.

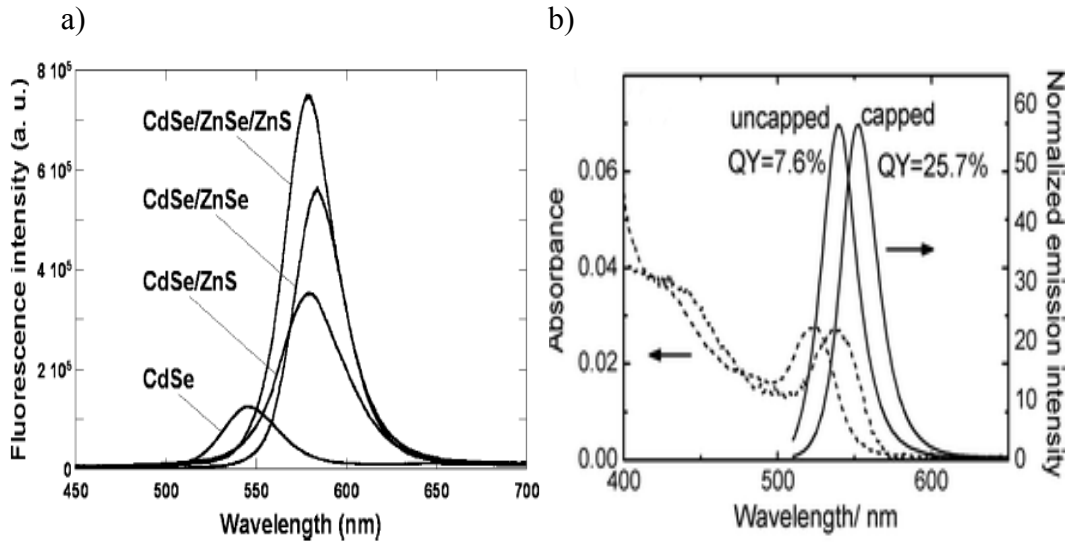

Figure 1.3. a) Photoluminescence spectra of CdSe nanocrystals before and after passivation with different types of inorganic semiconductor shells. (Source: Reiss, et al. 2003); b) Absorption and emission spectra of uncapped CdSe and ZnS capped CdSe QDs. (Source: Breus, et al. 2007)

The core-shell-shell nanocrystals were also developed, i.e., CdSe/CdS/ZnS (Talapin, et al. 2004), CdSe/ZnSe/ZnS QDs (Sun, et al. 2006). Double shell cause a better passivation of the core nanocrystal surface. The middle shell allows considerable strain relaxation between the inner core and the outer shell, and helps to further improve the fluorescence efficiency and photostability.

1.3.1. Classification of Core/Shell Systems

Depending on the relative position of electronic energy levels of the core and shell materials, two types;type-I and type-II, confinement regimes can be explained for core/shell QDs. The two types are illustrated in Figure 1.4.

In type-I core/shell QDs, the valence band edge of core is higher in energy than that of shell and the energy of conduction band edge of core is lower than that of shell, both the electron and hole are localized in the same region and can recombine very quickly, as shown in Figure 1.4.

In type-II regime, the energy of both valence and conduction band edges of core are higher than those of shell, the electron and hole are prone to being spatially separated between the core and shell for lower energy states.The regime results in longer lifetime of excitons before recombination (Reiss, et al. 2009) , as shown in Figure 1.4.

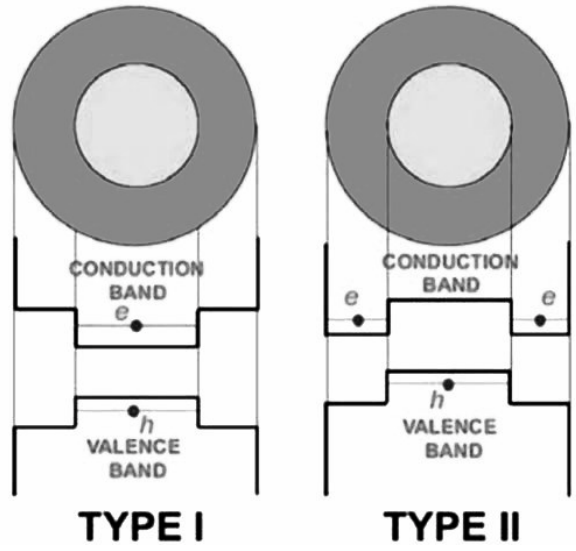

Figure 1.4. Schematic representation of the energy band alignment of type-I and type-II core/shell QD's. (Source: Tretiak and Piryatinski 2006)

The CdS/ZnS, ZnSe/CdS core/shell QDs are some examples of type I, and the CdSe/CdS, CdTe/CdSe, CdSe/ZnTe QDs are the examples of type II confinement regime.

1.4. $CdSe_xTe_{1-x}$ / CdS Core / Shell Quantum Dots

$CdSe_xTe_{1-x}$/CdS, an alloyed type core/shell nanocrystals, is not studied widely and still has terms to be developed. Core structure is called as alloy because both Te and Se precursors are added together at the same time during synthesis. However, because of the differences in reaction rates of Te and Se precursors, inner side of crystal structure is assumed to be Te or Se rich.

Nie et al. reported that in the alloyed semiconductor QDs (ternary CdSeTe), both the alloy composition (Se:Te molar ratio) and the internal structure can be controlled in a single step by varying the relative amounts of the starting materials.

After water solubilization, these alloy type QDs loses its fluorescence intensity and long term stability. To overcome this problem, Jiang et al. synthesized a CdS shell around $CdSe_xTe_{1-x}$ alloy-core by using organometallic route at very high temperature (325^0C) and they saw that the core shell nanoparticles had high quantum yield and narrow emission, near IR colored (Jiang, et al. 2006).

QDs with alloyed composition, are well suited for engineering materials with different electronic and optical properties, application in vivo molecular imaging and biocompetible materials for medical implants (Bailey and Nie 2003).

Piven et al. successfully synthesized water soluble $CdSe_xTe_{1-x}$ alloy type QDs by using short chain thiols as capping agent. The group adapts the method used by Rogach et al. in 1996, 1999 for synthesis of CdTe and CdSe respectively. NaHTe and NaHSe were used as tellurium and selenium precursors; thioglycolic acid was used as surface ligand. In their method, first Cd-thiolate complex formed in water and then Te/Se precursors were added respectively at 100^0C. At the end $CdSe_xTe_{1-x}$ nanocrystals with zinc-blend structure, which is characteristic for water soluble thiol stabilized CdTe and CdSe nanocrystals, were synthesized (Piven, et al. 2008).

1.5. Synthesis of Quantum Dots

Until now, different types of synthetic methods have been developed to produce nanocrystals. It is very important to grow monodisperse nanocrystals and to prevent dramatic drop in optical properties of these nanocrystals.

1.5.1. Organometallic Synthesis Method

Organometallic route, which is high-temperature synthesis in coordinating solvents in airless media provides tunable sizes and better surface passivation, improved by Bawendi, et al. 1993. Cadmium precursor and selenium, tellurium or sulfur precursors are dissolved in surfactant (TOPO or TOP generally) under nitrogen or argon atmosphere, at very high temperature (300^0C) nucleation occurs and by lowering temperature a little (280^0C), growth starts and monodisperse quantum dots forms.

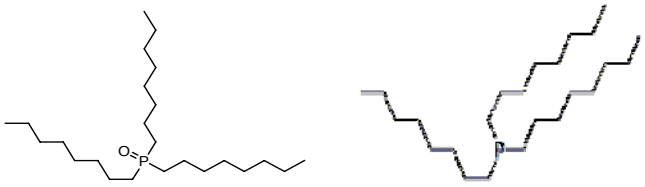

Figure 1.5. Structure of TOPO and TOP respectively

Trioctylphosphine oxide, TOPO, and Trioctylphosphine, TOP, (Figure 1.5.) are widely used organics in quantum dot synthesis, which function as both a solvent and as the stabilizing ligand. During the synthesis, functional groups of the ligands (phosphine oxides, phosphines and amines) bind to the QD surface, then the alkyl chains of the ligands leave direct away from the QD surface. As a model reaction path, the Figure 1.6 illustrates the growth of the CdSe NCs with addition of coordinated Cd and Se ions on the surface.

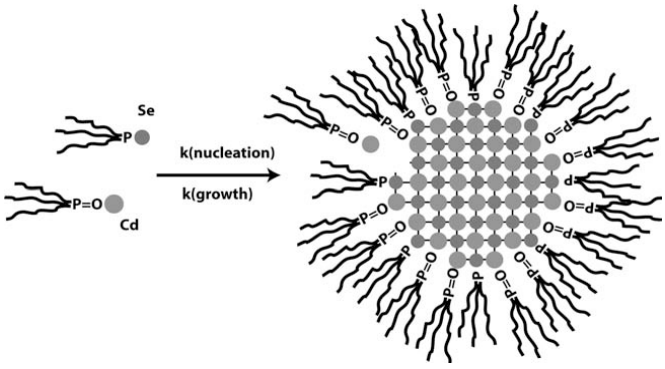

Figure 1.6. Model of a CdSe nanocrystal growing in a TOPO matrix due to the influx of Cd and Se ions selectively bound to an amphiphile molecule (TOPO and TOP).
(Source: Dushkin et al. 2000)

Talapin et.al synthesized CdSe / CdS nanoparticles via “greener” method using cadmium acetate as cadmium precursor (Talapin, et al. 2003). Capping the core with a higher band gap material, shell, like CdS removes the surface defects and improve fluorescence quantum yield (Smith, et al. 2004).

1.5.2. Two – Phase Synthesis Method

This method allows synthesis of quantum dots in low temperature and under atmospheric pressure. Cd precursor (Cadmium Myristate, synthesized from CdO and Myristic Acid) dissolves in oil phase (toluene or heptane) and Se or S precursor dissolves in aqueous phase and reaction occurs at interface of the two phases, as shown in Figure 1.7. Pan et al. synthesized CdS nanoparticles at atmospheric conditions at very low temperature (at 100^0C) corresponding to organometallic synthesis route (at 300^0C) (Pan, et al. 2004).

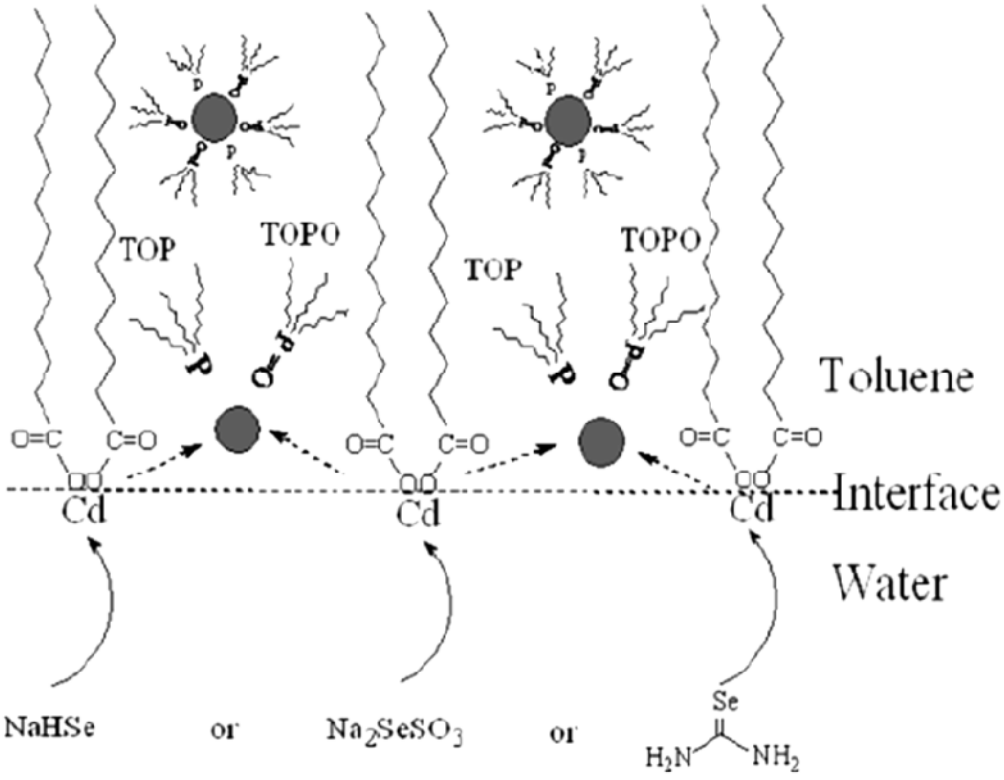

Figure 1.7. A proposed mechanism for formation of CdSe in oil phase
(Source: Pan, et al. 2007)

1.5.3. Aqueous Synthesis Method

Development of aqueous synthesis methods to produce less toxic quantum dots with high quantum yield, which is suitable for bioimaging applications, has been widely studied. These methods are simple, less expensive and more reproducible.

In recent years, the synthesis of QDs directly in water has been studied and Gaponik et al. synthesized photostable thiol-capped CdTe nanocrystals with quantum yield up to 40%. H_2Te gas (produced by the reaction of Al_2Te_3 - H_2SO_4) was used as Te precursors and passed through the solution together with nitrogen flow at 100^0C. Different thiol groups, such as,1-thioglycerol, 2-mercaptoethanol,thioglycolic acid, 2-mercaptoethylamine were used as capping agents (Gaponik, et al. 2002).

Rogach's group synthesized the citrate-stabilized CdSe nanocrystals in water at 70^0C with low quantum yield, at 0.1-0.15%, but size distribution was relatively narrow and the size distribution at fwhm was about 30-50 nm (Rogach, et al.2000).

Deng et al. also reported citrate-stabilized CdSe and CdSe/CdS nanoparticles synthesis method in aqueous solutions below 100^0C by bubbling the Cd-citrate-water solution with H_2Se and H_2S gases as selenium and sulfide precursors, Figure 1.8. They incorporated a photoactivation procedure by putting the nanoparticles under ambient light for a few days. They hypothesized that this would eliminate topological surface defects and QY increased, reporting a final QY of 4%. (Deng, et al. 2006).

Peng et.al described a one pot synthesis method for CdTe/CdS nanoparticles using thioglycolic acid (TGA) as capping agent (Peng, et al. 2007). Gu et.al synthesized 3–mercaptopropionic (3-MPA) acid capped CdTe/CdS nanoparticles and obtained highly luminescent by using NaHTe as Te precursor (Zhong, et al. 2008).

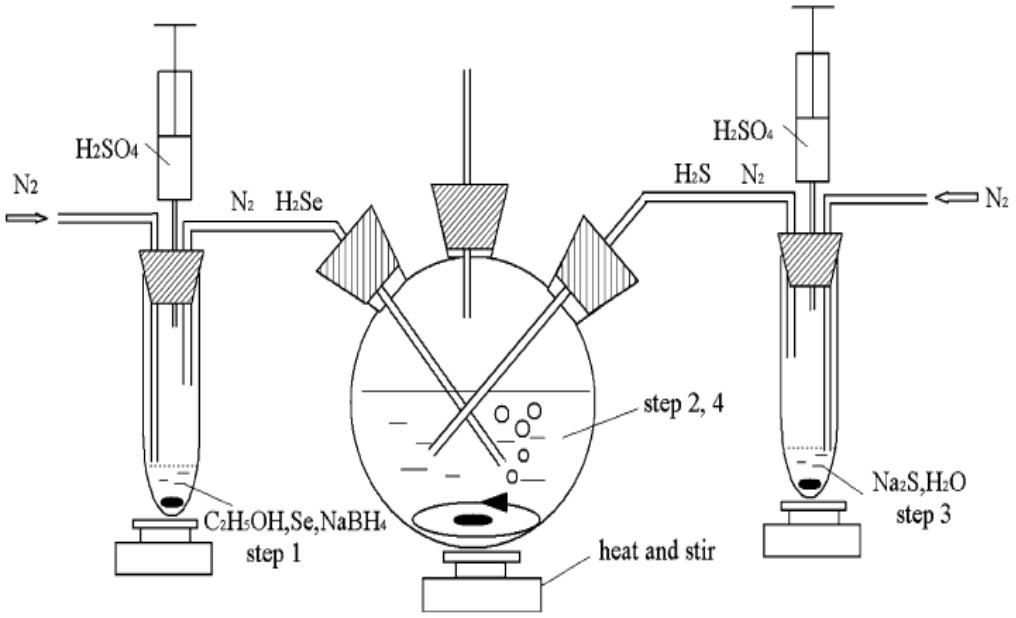

Figure 1.8. Schematic presentation of the synthetic route of water-soluble CdSe and CdSe/ CdS NPs. (Source: Deng, et al.2006)

Maysinger et al. modify the cysteamine capped CdTe QD surface with an antioxidant, N-acetylcysteine (NAC), to have less cytotoxic nanoparticles for using in cancer research. NAC covalently bind to cysteamine on the CdTe QD surface (Figure 1.9) and NAC-conjugated CdTe QDs prodeced, thus net surface charge decreased. As a result of charge-charge complexation of NAC with cysteamine formed NAC-capped CdTe QDs with carboxylic groups on the surface.

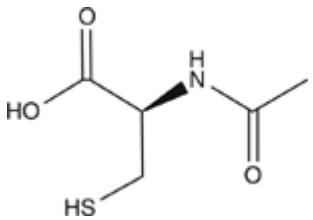

Figure 1.9. Structure of N-acetylcysteine (NAC)

Liu et al. synthesized 3-MPA stabilized CdTe and to accelerate the growth of CdTe QDs, they chosed one kind of chemical reagent rather than heat or radiation. Because the hydrogen telluride is sensitive to oxygen in the solution, they used hydrazine hydrate as reducing reagent to protect HTe^- to get high quality CdTe QDs.

QDs grown at room temperature, after 6 h, the PL QY reached the maximum value of 62%.

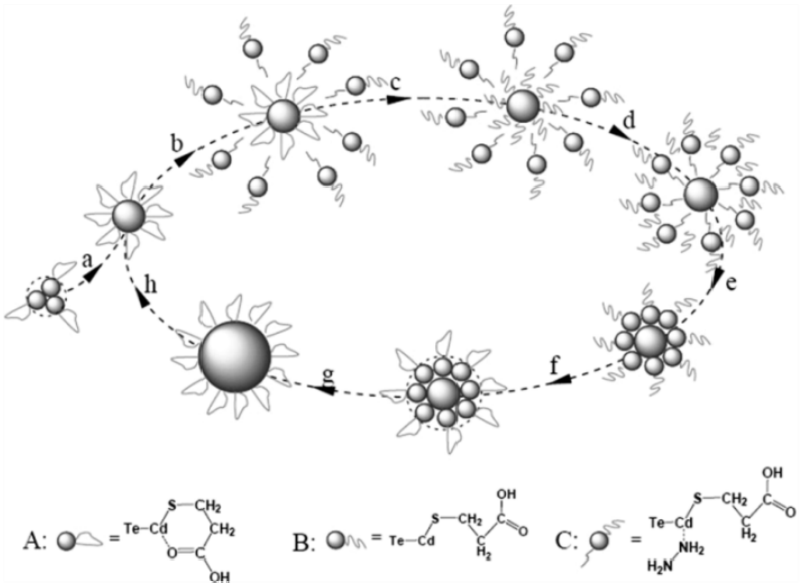

Figure 1.10. The hypothetical growth of CdTe NCs initiated by hydrazine hydrate. (Source: Liu et al. 2008)

Growth mechanism was illustrated with the schematics in Figure 1.10. Several CdTe molecules clustered together into a crystal nucleus shown in Figure 1.10-a; the complex between cadmium monomers and MPA, and than NH_2–NH_2 is close to the crystal nucleus shown in Figure 1.10-b; the other side of NH_2–NH_2 reacts with cadmium of the crystal nucleus and is replaced the position of oxygen in MPA (Figure 1.10-c and d); NH_2–NH_2 divorces from the surface of CdTe after cadmium monomers deposited on it (Figure 1.10-e); MPA is chelated with CdTe NCs as before and a CdTe crystal nucleus grew on the NCs successfully (Figure 1.10-f and g), and the CdTe NCs continually grows in this way cyclically (Figure 1.10-h) (Liu, et al. 2008).

1.5.4. Microwave Synthesis Method

Short reaction times, lower reaction temperatures and ambient atmospheric conditions during reaction are the advantages of microwave synthesize method, but this method was generally used to have hydrophobic QDs. Microwave power and

temperature are critical in producing the highest structural, monodisperse, and optically qualified crystals.

Wang et al. synthesized CdSe and CdSe/CdS semiconductor QDs by using sodium citrate as a stabilizer. They heated the precursors in microwave oven (900 W) for 50s. To obtain biocompetible semiconductors, they used silica shell encapsulation method. Quantum yield was increased after certain illuminationin in presence of oxygen and after photoactivation process. Core CdSe QDs had QY of up to 20%, compared to 0.01-0.43% QY at the beginning state. (Wang, et al. 2004)

Ziegler et al. synthesized tri-n-octylphosphine oxide (TOPO), hexadecylamine (HDA) capped CdSe/ZnS QDs which have emission wavelengths between 580 to 635 nm with 50% quantum yield. During synthesis microwave was operated at 2.44 GHz, with 800 W power with 200^0C temperature (Ziegler, et al. 2007).

Strouse and co-workers synthesized CdSe and CdTe nanocrystals by using solvents of different alkyl chain lengths (CdSe 5s-10 min, CdTe 5s-1 min) and they operated the microwave at 300 W, 2.45 GHz. Cadmium stearate (CdSA) ,TOP-Se and TOP-Te were used as starting materials (Washington and Strouse 2008).

1.5.5. Hydrothermal Synthesis Method

As the temperature of liquid water increases, the static dielectric constant decreases, also hydrogen bonding and surface tension become less pronounced. A lower surface tension increases wettability, and when coupled with the high temperature water, could effectively anneal the surface of the nanocrystal and reduce the number of surface defects (Geens, et al. 2005).

Adschiri group (2001) and Arai group (2003) synthesized nanocrystalline metal oxides by using high-temperature water. Crystal size and crystal structure can be controlled by changing temperature, reaction time and pressure (Arai, et al. 2003).

Zhao et al. synthesized water-soluble near-infrared emitting CdTe/CdS QDs in aqueous solution by using thiol ligand N-acetyl-L-cysteine (NAC) as capping agent, via a one step hydrothermal route. $CdCl_2$ and NAC were dissolved in 40 mL water and the NaHTe precursor solution was added, then solution was loaded into a 40-mL Teflon-lined stainless steel autoclave and incubated in an 200^0C oven for 53-69 min. The synthesized QDs had 45-62% quantum yields(Zhao, et al. 2009).

1.6. Water Solubilization of Quantum Dots

For biomedical applications, quantum dots synthesized via organometallic route must be modified. Different methods can be used to make hydrophobic QDs biocompetible.

In 1998, Alivisatos et al. and Nie et al. confirmed that semiconductor QDs could be made water soluble and conjugated via biological molecules.

1.6.1. Ligand Exchange Method

Ligand exchange method is widely used to make QDs water soluble. First oil soluble quantum dots with high quantum yield was synthesized, and then hydrophobic surfactant was replaced with a hydrophilic surfactant which can be dissolved in water, as shown in Figure 1.12.

3 – Mercaptopropionic acid and Thioglycolic acid are commonly used capping agents in ligand exchange procedures (Figure 1.11). These capping agents bind quantum dots' surface from thiol group (-SH) and free carboxylic groups (-COOH) facing the solution, this allow 3-MPA or TGA capped quantum dots to be able to dissolve in aqueous media.

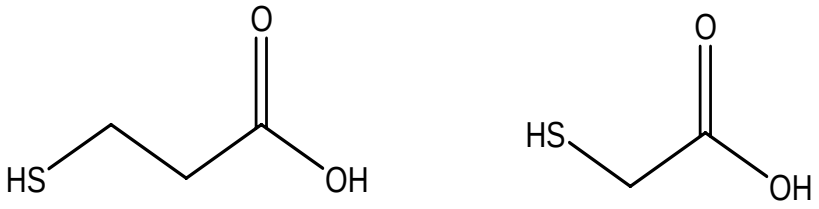

Figure 1.11. 3 – Mercaptopropionic acid and Thioglycolic acid, respectively.

After ligand exchange surface modification, surface defects in crystal structure mostly present and quantum yield of quantum dot may reduce.

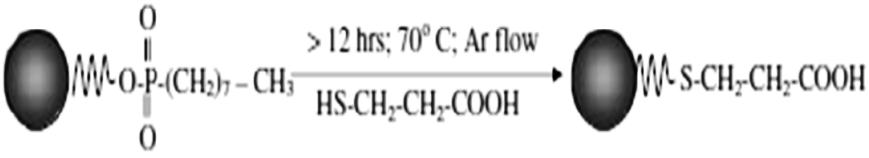

Figure 1.12. A schematic depicting water repelling ends (TOPO) substituted with hydrophilic ends (-COOH group in MPA) (Source: Kumar, et al. 2008)

1.6.2. Surface Silanization Method

In surface silanization, silane groups can be polymerized into a silane shell around the QDs. Silanization of the NC surface was widely used in particular by the Alivisatos group. This method requires multiple-time consuming steps.

Functional organosilicone molecules containing $–NH_2$ or –SH, are incorporated into the shell and provide surface functionalities for biomedical applications.

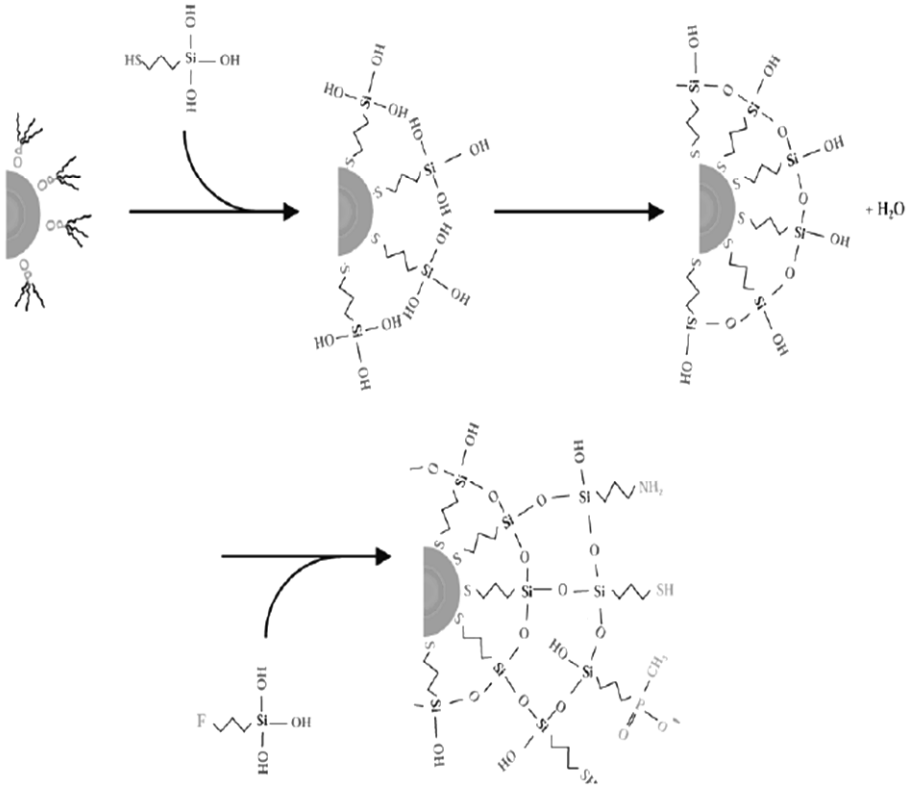

Figure 1.13. Schematic of SiO2 capping of CdSe/ZnS structure with various functional groups (Source: Gerion, et al. 2001).

Gerion et al., from Alivisatos's group, reported a method of SiO_2 capping of ZnS capped CdSe quantum dots using silane precursors to form a network of siloxane bonds around the individual CdSe particles and eventually producing a SiO_2 shell. Figure 1.13 shows a schematic of the shell structure they proposed. Silica coating needs to be carried out at dilute conditions, which does not permit large quantity fabrication (Gerion, et al. 2001).

1.6.3. Encapsulation Amphiphilic Phospholipid Micelles

In a QD micelle synthesis procedure, a concentrated suspension of QDs in chloroform is added to an aqueous solution containing a mixture of surfactants or phospholipids with different functional head groups such as ethylene glycol (-PEG) and amine ($-NH_2$).

PEG is used to improve biocompatibility and amine groups provide sites for bioconjugation. The formation of a micelle with trapped TOPO-capped CdSe nanoparticles is shown by the schematic in Figure 1.14. Hydrophobic alkyl end of TOPO capped CdSe which binds to the hydrophobic end of the surfactant and its hydrophilic –COOH/–OH group make it biocompatible in the aqueous media (Kumar, et al. 2008).

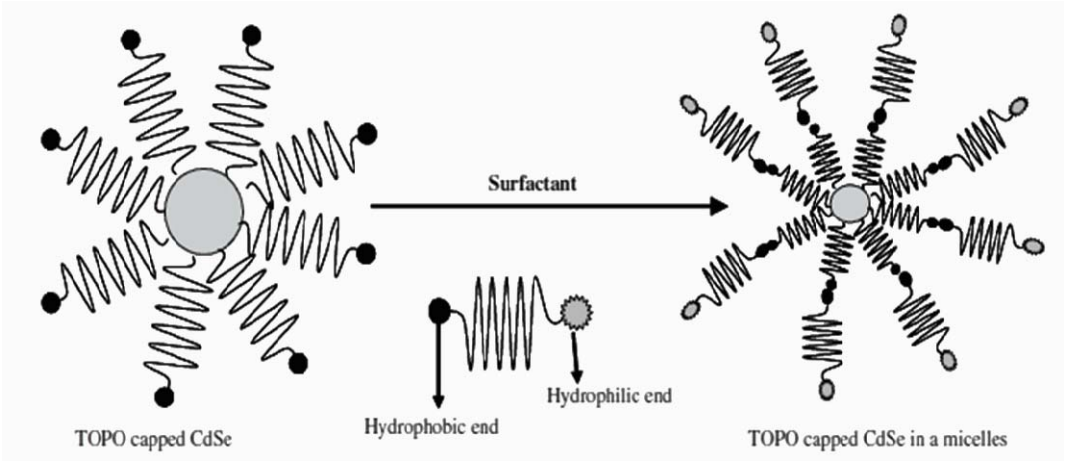

Figure 1.14. Schematic showing the formation of a micelle with trapped TOPO-capped CdSe nanoparticles (Source: Kumar, et al. 2008).

1.7. Characterization Techniques

Characterization is the most important part of the research, which give us information to understand the structure and composition of synthesized materials. Characterization techniques of nanoparticles can be divided into two as optical characterization and structural characterization.

Our purpose was to synthesize nanosized semiconductor crystals and to control their size-tunable optical characteristics, so Fluorescence and UV – Vis Spectrometries are widely used to characterize nanocrystals' optical properties.

X – Ray Diffractometer (XRD) are generally used for defining crystal structure of quantum nanocrystals because, each crystalline material has its own characteristic X-Ray diffraction powder pattern.

As a microscopic techniques, Transmission Electron Microscopy (TEM) can be used to help the structure determination and Scanning Electron Microscope (SEM) coupled with the energy dispersive x-ray detector (EDX) can be used to determine the chemical composition of a nanocrystal. Also, elemental analysis can be carried out via Inductively Coupled Plasma Mass Spectroscopy (ICPMS) .

Toxicity is a very important property when the synthesized QDs are used in biological applications. MTT and Trypan blue tests can be performed to determine toxicity of quantum dots. At last confocal microscope can be used in bioimaging applications.

1.7.1. Spectroscopic Characterization

Quantum dots have unique optical properties, thus their characterization should be carried out carefully. Fluorescence and UV – Vis spectrometers are used to determine optical properties of QDs.

1.7.2. UV-Vis Absorption and Fluorescence Spectroscopy

Spectroscopic properties are related with the size and the elctronic structure. As the band gap increases by decreasing the particle size, then absorption shifts from infrared to visible region.

By reducing the particle size, absorption shifts to higher energies and different allowed possible transitions results in different discrete bands due to the size dependent quantum confinement.

QDs have Gaussian shaped sharp emission peaks, small Stokes shift can be observed via the recombination of electron hole pairs. Figure 1.15 shows typical absorption and fluorescence spectra of CdSe nanocrystals in colloidal solution.

Stokes shift is the difference between band maxima of fluorescence and absorption spectra of the same electronic transition. This difference is the result of a combination of relaxation into shallow trap states and the size distribution

Stokes shift ($\Delta\upsilon$) can be calculated with this formula;

$$\Delta\upsilon = \upsilon_{absorbance} - \upsilon_{fluorescence} \quad (1.1)$$

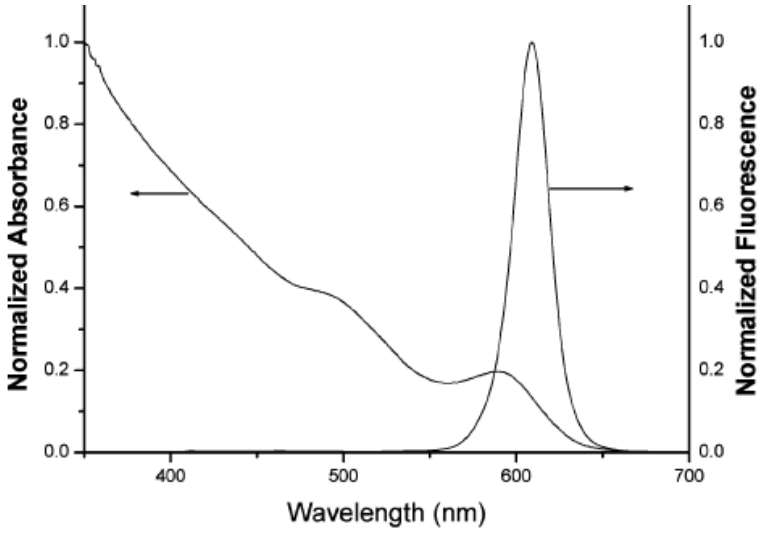

Figure 1.15. Normalized linear absorbance and PL spectra of TGA-capped CdSe-ZnS core-shell quantum dots in solution. (Source: Wang, et al. 2006)

In absorption of a quantum of light, an electron is excited from valence band to conducton band energy levels over the band gap (excited states). This is followed by a very fast nonradiative vibrational relaxation process, which brings the electron to the lowest excited state in conduction band. This process can be followed by fluorescence emission, the system emits a photon (fluorescence) and relaxes to the ground state in

valence band. During relaxation of electron, the trapping of electrons and holes by trap states within band gaps can cause alternative pathways (Figure 1.16).

At longer wavelength, broader bands can be observed for particles consisting of surface defect states, and this leads to quenching of the band gap emission and appearance of weak deep trap long-wavelength emission.

The width of the peak, typically reported as the full-width-at-half-maximum (FWHM), is generally used to appraise the particle size distribution, in other words, FWHM is used to determine monodispersity of quantum dots.

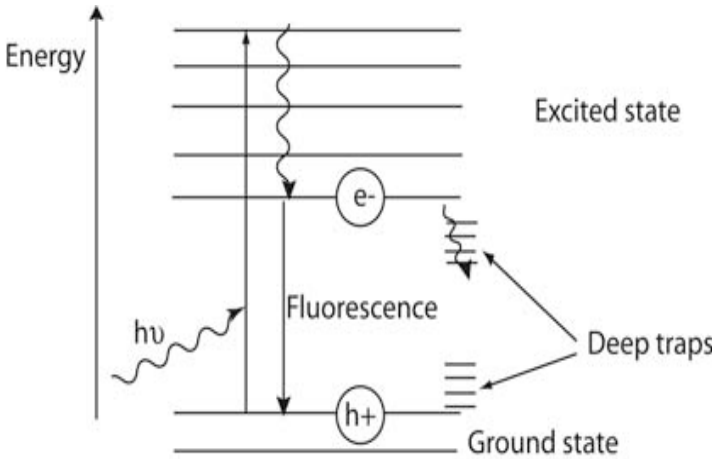

Figure 1.16. Schematic path for absorption of light, vibrational relaxation and fluorescence emission or relaxation through trap states. (Source: Klimov, et al. 2000)

1.7.2.1. Measurement of Quantum Yield (QY)

The fluorescence quantum yield is the ratio of the number of emitted photons to the number of absorbed photons. The quantum yield is then calculated by using the Equation (1.2.).

$$QY_{QD} = QY_{dye} \frac{I_{QD}}{I_{dye}} \frac{OD_{dye} n_{QD}^2}{OD_{QD} n_{dye}^2} \quad (1.2)$$

where QY is the quantum yield, $n_{QD,dye}$ is the refractive index, $I_{QD,dye}$ is the integrated fluorescence signal for the QD and dye solutions and $OD_{QD,dye}$ is the absorbance of QD and dye at the excitation wavelength respectively.

1.7.3. Structural Characterization

Structural characterization of semiconductor nanoparticles can be determined X–Ray Diffractometer (XRD) and Transmission Electron Microscopy (TEM).

1.7.3.1. X-ray Diffraction

X-ray diffraction (XRD) technique is useful for investigating the crystal structure of a solid with lattice constants and geometry. By comparing hkl indexes of bulk and nano structures, unknown crystal structure and size can be determined. Depending upon synthesis method, CdTe and CdSe QDs have been reported either wurtzite or zinc-blende structure. (Figure 1.17). The structure of individual dots depends on the growth mechanism, applied pressure and temperature.

Both structure types share the same immediate atomic ordering where each metal (Cd) and nonmetal (Se/Te) atom is tetrahedrally coordinated by unlike atoms. Their crystallographic symmetry is different, zinc blende has cubic structure and wurtzite has hexagonal structure.

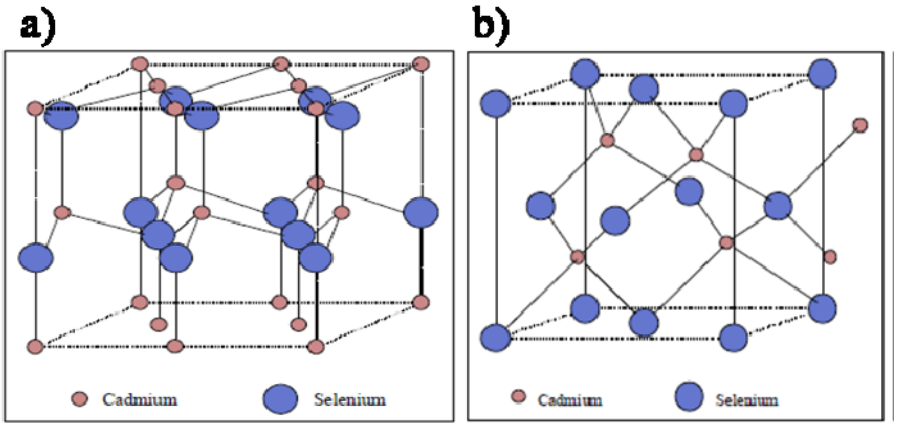

Figure 1.17. a) Schematic of wurtzite structure, b) schematic of zinc-blend structure.

Also, core and core shell crystal structure can be determined by using XRD through observing peak shifts in XRD spectrum, (Figure 1.18).

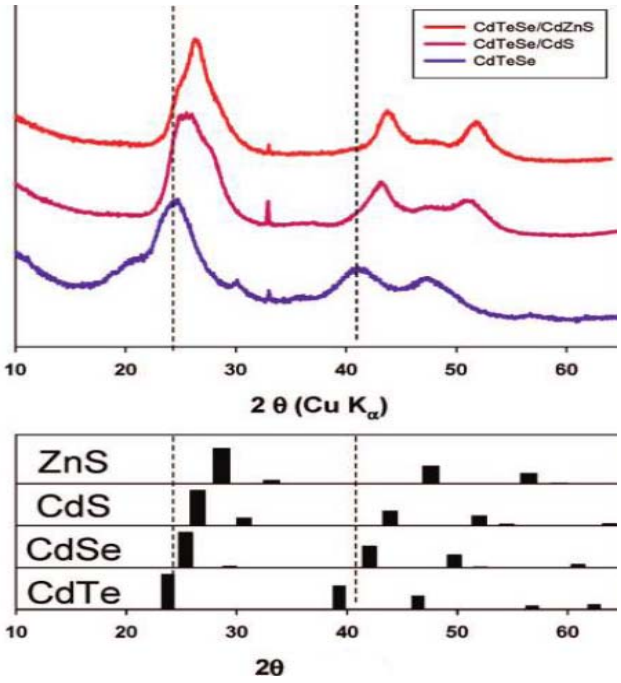

Figure 1.18. Top: X-ray diffraction patterns from (bottom to top): CdTeSe, CdTeSe/CdS, and CdTeSe/CdZnS QDs. Bottom: Theoretical X-ray diffraction patterns for bulk zinc blende CdTe, CdSe, CdS, and ZnS. Dashed lines are guidelines for the eyes. (Source: Pons, et al.,2009)

X-rays are produced by colliding a high speed electron with a metal target under the high voltage system. Produced X-ray beams fall on a specimen, then they are diffracted by the crystalline phases in the specimen according to the Bragg's law shown in Equation (1.3).

$$n\lambda = 2d\sin\theta \tag{1.3}$$

where n is the order, λ is the wavelength of X – Rays, d is the interplanar spacing between planes in the atomic lattices and θ is the angle between incident beam and scattering plane.

Average crystallite size (D) can be estimated by using x-ray diffraction pattern with applying Debye Scherrer's equation (Equation (1.4.)):

$$D = \frac{0.9\lambda}{B\cos\theta_B} \tag{1.4}$$

where D is the diameter of the nanocluster, λ the wavelength of the incident X-rays, B is the full-width at the half-maximum of the Bragg peak , and θ_B is the diffraction angle.

The compositions of nanocrystals can be estimated from XRD - pattern by applying Vegard's law (Equation (1.9)).For hexagonal structures crystal growth occurs in c-axis but for cubic structures growth of crystal occurs in a – axis.

For Hexagonal structures;

$$\frac{1}{d^2} = \frac{4}{3}\left(\frac{h^2 + hk + k^2}{a^2}\right) + \frac{l^2}{c^2} \tag{1.5}$$

For Cubic structures;

$$\frac{1}{d^2} = \left(\frac{h^2 + k^2 + l^2}{a^2}\right) \tag{1.6}$$

by combining these equations and Bragg's law (Equation (1.3)), a is represented as;

$$a = \frac{n\lambda}{2\sin\theta}\sqrt{h^2 + k^2 + l^2} \tag{1.7}$$

Most intense XRD peak can be used to calculate a,where n is1and λ is 1.54 A,

$$a = \frac{1.33}{\sin\theta}\ \text{A} \tag{1.8}$$

By using Vegard's law (Equation (1.9)) mole ratios of alloy CdSeTe nanocrystals which have cubic structures can be calculated,

$$a(x) = x\ .\ a_{\text{CdSe}} + (1 - x)\ .\ a_{\text{CdTe}} \tag{1.9}$$

where x is mole ratio and a is lattice parameters.

1.7.4. Transmission Electron Microscope

Transmission electron microscope (TEM) is commonly used technique to investigate the nanocrystals morphology, because objects can seen to the order of a few angstrom.

In TEM, electrons are used as light source, because their lower wavelength makes it possible to get a better resolution than a light microscope. A light source emits the electrons then the electrons travel through vacuum in the column of the microscope. Electromagnetic lenses are used in TEM to focus the electrons into a very thin beam; this beam then travels through the specimen. The unscattered electrons hit a fluorescent screen at the bottom of the microscope and depend on the density; different parts of the specimen can be displayed in varied darkness. The observed image can be photographed with a camera.

Crystal structure, size dispersity of synthesized nanocrystals can be determined by using TEM (Figure 1.19).

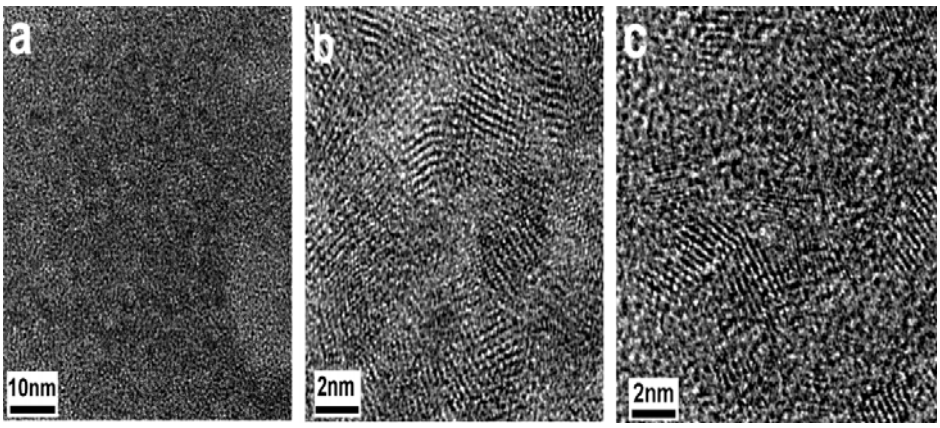

Figure 1.19. Typical TEM overview of alloyed $CdSe_xTe_{1-x}$ NCs a), and HRTEM images of CdSe(0.1)Te(0.9) b), and CdTe c) NCs grown for 24 h.(Source: Piven, et al. 2008)

1.8. MTT Test

Because the QDs contain toxic elements such as cadmium and selenium, they should be tested before used in live cells. Cd cause cell death via mitochondrial damage and oxidative stress (Drezek, et al. 2008). Capping QDs via hydrophilic shells makes them non-toxic. However, if the surface coating is not stable or CdSe exposed oxidation

then, Cd^{2+} released and QDs become toxic, this makes them unfavored for live cell experiments. Many research groups study dependence of cell deths with higher concentrations (Alivisatos, et al. 2005).

Toxicity of nanocrystals can be determined by MTT assay, which is a quantitative colorimetric test, and by the assay the color change is observed in living organisms. MTT test works based on the action of mitochondrial dehydrogenases of cells that cleave the tetrazolium ring of yellow colored 3-(4,5-Dimethylthiazol-2-yl)-2,5-diphenyltetrazolium bromide (MTT) and forming purple formazan crystals (Burgess, et al. 2006).

By comparing the change in metabolic activity of cancer cells, before and after injection of QDs gives us information about cytotoxicity of nanocrystals.

1.9. Confocal Microscopy

The confocal microscope has been used for alive or fixed cell imaging (Figure 1.20). Quantifying the temporal dynamics of the intermittent fluorescence typical of nanocrystals yields information on their electronic structure, and the fast on-off fluorescence can be captured with high speed optical detectors, like the photomultiplier tube (PMT) or the avalanche photodiode (APD), attached to the confocal.

By splitting the light coming back from the sample, sending half to an APD and the remainder through a prism onto a CCD, high resolution time and spectral data can be collected simultaneously.

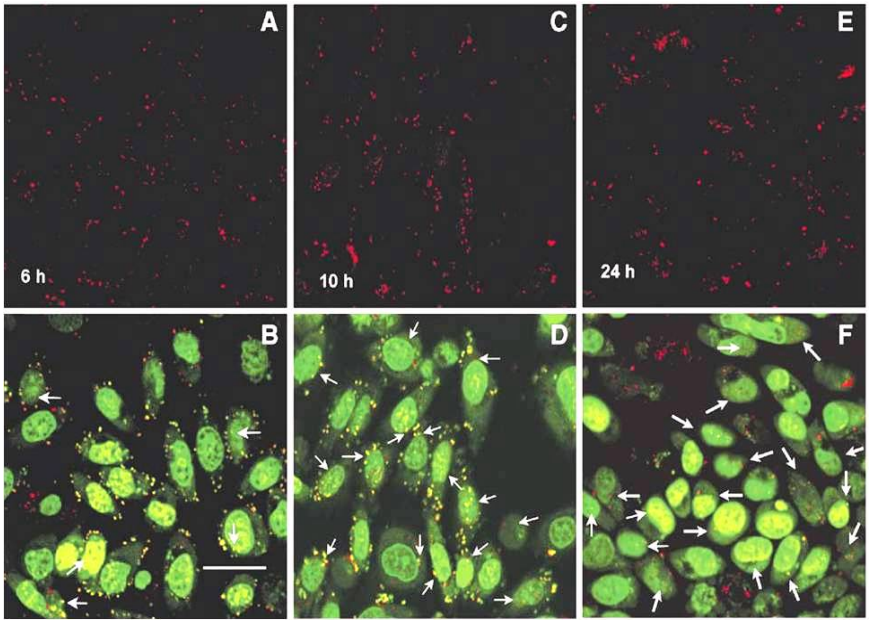

Figure 1.20. Confocal images following incubation with QD–DNA conjugates at different time. Cells were stained with SYTO-16 nuclear stain. a), c), and e) are photomicrographs of the red channel for the QD–DNA conjugate and b), d), and f) are micrographs showing the overlapped images of the green and the red channels. (Source: Burgess, et al. 2006)

1.10. Biological Applications of Quantum Dots

Semiconductor nanocrystals can be widely used in biological applications because of their unique optical properties. In the early stages, QDs were commonly used in imaging applications in stead of organic dyes. After the observation that QDs kept on emitting fluorescent light for weeks the brilliant potential of these materials was realized. This was advancement for microscopic imaging, which helped in unfolding many cellular processes. Different compositions of the same material but of different sizes had been made, which can generate different colors after excitation by light of a single wavelength. It was then confirmed that QDs tagged with biomolecules such as antibodies, peptides etc. can be employed to detect specific molecules on the cell surface or inside the cell (Vashist, et al. 2006).

Nanocrystals have some favorable futures compare to organic dyes. Molar extinction coefficient of QDs 10 to 50 times larger than organic dyes thus, absorption rates are faster. QDs have large absorption cross section which allows wide wavelength selection and straight excitation and emission separation. QDs show size-tunable fluorescence emission compared to organic dyes, this makes them ideal for

simultaneous detection of multiple fluorophores by excitation of a single light source (Kotov, et al. 2005)

They have higher photoluminescence quantum yield, also they are more stable against photobleaching than organic dyes. QDs have low photo-degradation rates, this make continuous or long-term monitoring of slow biological processes possible (Gengeret, al. 2008)

QDs are larger than organic dyes in size, when multicolor experiments required in biomolecules with QDs of different sizes, this can result in some complication due to the large differences in the QD sizes. Because organic dyes have poor photostability and low quantum yields in biological media, QDs are a desirable alternative (Bailey, et al. 2004).

1.10.1. Immunofluorescence Labeling

Alivisatos' group used TOP/TOPO capped CdSe/ZnS QDs in multicolor labeling of fixed mouse 3T3 fibroblasts. They used silica shell to make QDs water soluble, then biotinylated QDs with red photoluminescence selectively stained cytoskeletal filaments modified with streptavidin. Green-emitting QDs with acetate groups showed high affinity to the cell nucleus (Bruchez, et al. 1998).

Chan and Nie prepared water soluble CdSe QDs by exchanging organic ligand with mercaptoacetic acid, that were labeled with the protein transferrin underwent receptormediated endocytosis in cultured HeLa cells, and those QDs were labeled with immunomolecules recognized specific antibodies or antigens. (Chan, et al. 1998).

Dahan group linked the glycine receptor (GlsRs) to QDs through primary antibody and secondary fragment bridges then studied dynamics in neuronal membranes. They analyzing the trajectories then obtained localizations and diffusion coefficients (Dahan, et al. 2003).

Ness group used QDs in immunohistochemical process to detect intracellular antigens in rat and mouse brain tissues. Their study showed that QD immunohistochemical labeling is more sensitive than immunohistochemical approaches using organic dyes (Ness, et al. 2003).

1.10.2. In Vivo Imaging

Semiconductor QDs also were used as tagging agent for in vivo imaging of prelabeled cells. Akerman group first reported the use of QD–peptide conjugates to target receptors on blood vessels with exquisite binding specificity. This work demonstrates the feasibility of in vivo targeting, but not of in vivo imaging (Akerman, et al. 2002).

Another group, Debertret et al. reported the microinjection of phospholipid coated QDs into xenopus embryos to study the behaviour of embryogenesis (Debertret, et al.2002). Microinjection technique is a very strenuous technique that does not allow high volume analysis.

Gao group reported a new class of multifunctional QD probes for targeting and imaging of tumors in live animals. The structural design involves encapsulating luminescent QDs with an amphiphilic triblock copolymer, and linking this amphiphilic polymer to tumor-targeting ligands and drug delivery functionalities. In vivo targeting studies of human prostate cancer growing in nude mice indicate that the QD probes can be delivered to tumor sites by both enhanced permeation and retention and through antibody binding to cancer-specific cell-surface biomarkers (Gao, et al. 2004).

There are some difficulties in animal body imaging. The main difficulty is toxicity of quantum dots and also autofluorescence of tissues is another difficulty in fluorescence tissue monitoring. Tissue autofluorescence minimizes in near infrared region (700 – 1000 nm) and fabricating quantum dots that emit light in near infra red region can solve this problem.

Still, the cellular toxicity and in vivo degradation mechanisms of QD probes need to be studied. In vivo toxicity is an important criteria in determining if the QD imaging probes would be approved by regulatory agencies for human clinical use.

CHAPTER 2

SYNTHESIS AND CHARACTERIZATION METHODS OF CdSeTe BASED NANOPARTICLES

2.1. Experimental Procedure

Synthesis of water dispersible alloyed CdSeTe nanocrystals was carried out by a modified method reported by Piven et al. $CdSe_xTe_{1-x}$ /CdS nanocrystals were stabilized with short-chain thiols as a ligand (Piven, et al. 2008).

2.1.1. Synthesis of NaHSe as Se and NaHTe as Te Precursor

Aqueous solutions of NaHSe and NaHTe as selenium and tellurium precursors were prepared respectively, under N_2 atmosphere. Precursors were prepared by reduction of powders of elemental Se and Te with $NaBH_4$ according to the following reactions:

$$4\ NaBH_4\ (aq) + 2\ Se(s) \rightarrow 2\ NaHSe\ (aq) + Na_2B_4O_7(s) + 14\ H_2(g)$$
$$4\ NaBH_4\ (aq) + 2\ Te(s) \rightarrow 2\ NaHTe\ (aq) + Na_2B_4O_7(s) + 14\ H_2(g)$$

To prepare the Se precursors, Se powder (0.026 mmol, 2.05mg) and $NaBH_4$ (0.05 mmol, 1.9mg) were put into a reaction flask under N_2 atmosphere and 2.0 ml of ultra pure water was added to the reaction flask. Resulting clear solution of NaHSe was obtained with a side product of $Na_2B_4O_7$ formed at the bottom of the sealed vial in1 hour, at room temperature.

The Te precursor was prepared by mixing Te powder (0.15 mmol, 19.2mg) and $NaBH_4$ (0.3 mmol, 11.4mg) in a reaction flask under N_2 atmosphere.Then 2.0 ml of

ultra pure water was added to the reaction flask and the flask was heated to 80^0C. Resulting dark-purple NaHTe solution was obtained in 2 hours, at 80^0C (Figure 2.1).

Because both NaHSe and NaHTe are very sensitive to air, freshly synthesized precursor solutions were used in all experiments, without any purification.

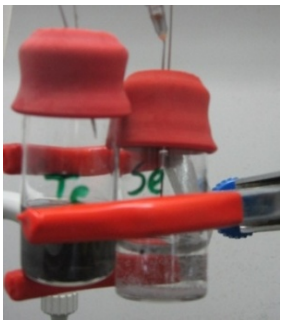

Figure 2.1. Schematic representation of resulting NaHTe and NaHSe solutions, respectively.

2.1.2. Synthesis of $CdSe_xTe_{1-x}$ Nanoparticles

First, 0.58 mmol (0.1076g) $CdCl_2$ was dissolved in 40ml ultra pure water and 0.93 mmol (66µl) surface ligand thioglycolic acid (TGA) was added was added to the solution under stirring. pH of the solution was adjusted to 11.5 by addition of 1.0 M NaOH. Reaction was performed under N_2 atmosphere and vigorous stirring. Temperature was set 90^0C and 100^0C as optimization parameters. Cd - thiolate complex was formed in 1 hour.

2.0 ml of freshly prepared solution of NaHSe and freshly prepared solution of NaHTe were simultaneously injected into the nitrogen-saturated, vigorously stirred Cd-thiolate complex by the help of two syringes. NaHSe solution prepared by using 0.026 mmol (2.1 mg) Se-powder, 0.052 mmol (1.9 mg) $NaBH_4$ in 1 ml ultra pure water, under N_2. NaHTe solution prepared by using 0.15 mmol (18.8 mg) Te-powder, 0.30 mmol (11.4 mg) $NaBH_4$ in 1 ml ultra pure water, at 80^0C under N_2.

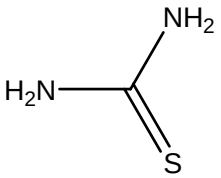

Figure 2.2. Structure of thiourea

Formation of water dispersed TGA capped $CdSe_xTe_{1-x}$ particles can be accompanied by the change of appearance of the solution from colorless to dark red under the day light (Figure 2.3). After the synthesis of CdSexTe1-x nanocrystals, following the addion of Se/Te precursors, sulfur source which was prepared by dissolving 0.26 mmol (19.8 mg) thiourea in 2.0 ml water was added to the sotution of CdSexTe1-x nanocrystals (Figure 2.2) to coat the core nanocrystals.

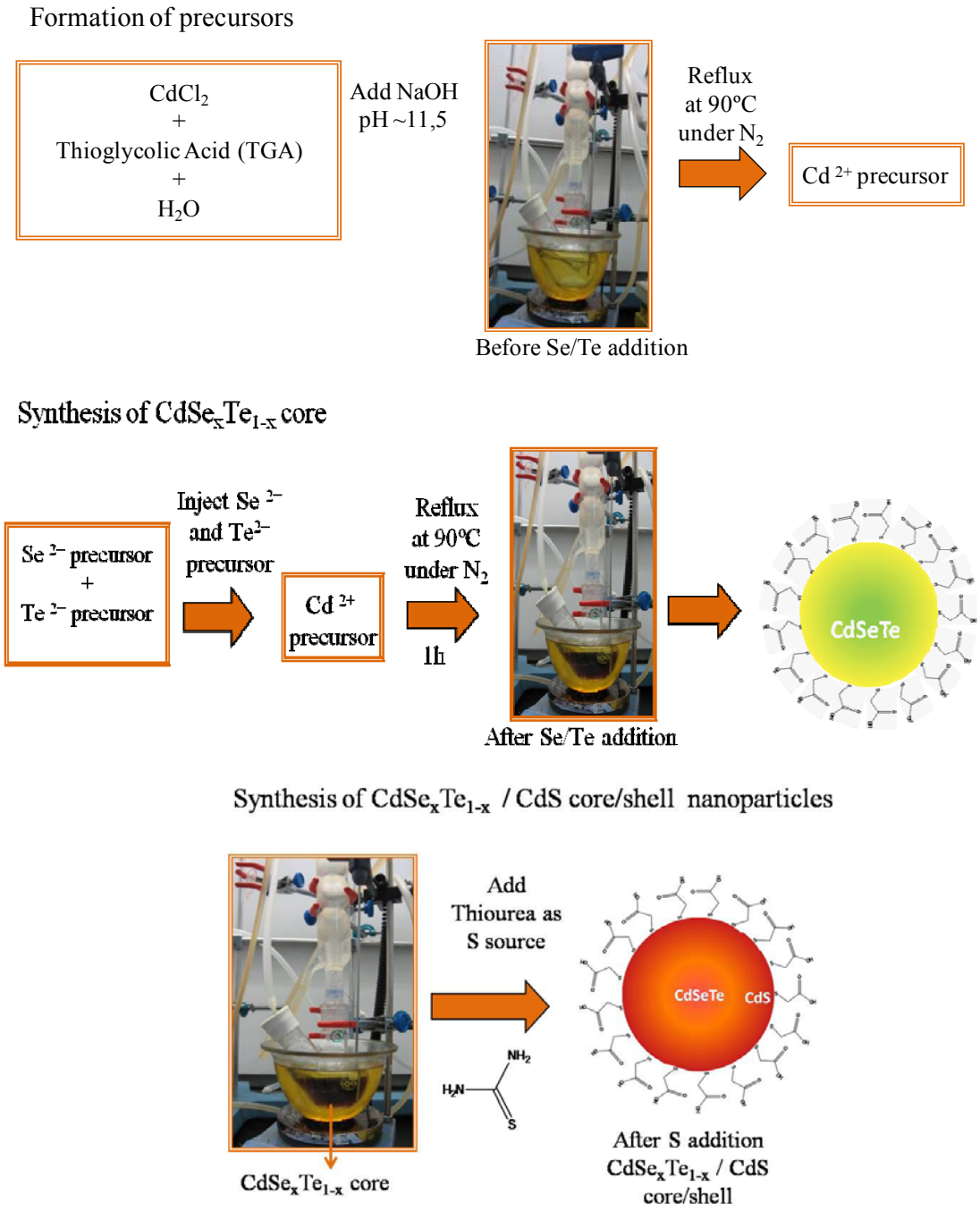

Figure 2.3. Schematic representation of water dispersed synthesis of $CdSe_xTe_{1-x}$/CdS.

Aliquots from reaction flask at different time intervals were taken to monitor the formation of nanoparticles by using UV – Vis and fluorescence spectroscopy. Reaction was stopped by cooling the solution to room temperature when the size of nanoparticles was reached to desired size. Nanoparticles were precipitated by addition of the 2-propanol in to the crude solution and centrifugation was performed at 6000rpm. Precipitated nanoparticles were then dried at room temperature.

In order to optimize optical properties of nanoparticles, mole ratios of Cd/TGA and Se/Te precursors were varied and CdSeTe/CdS nanocrystals with better crystal structure and higher quantum yield were obtained by this optimization. Optimization conditions were summarized in the Table 2.1.

Table 2.1. Experimental information of CdSeTe/CdS nanocrystals synthesis.

CODE	MOLE RATIO Cd:TGA	MOLE RATIO Cd:(Se+Te)	MOLE RATIO Te:Se	MOLE RATIO Se : S	pH	Temp. (^{0}C)	Reaction Volume (ml)
A1 : CdSeTe-*Core*	1 : 2.4	1 : 0.3	0.5:0.5	*No thiourea*	11.2	100	120
A2 : CdSeTe/CdS	1 : 2.4	1 : 0.3	0.9:0.1	1:10	12.1	100	40
A3 : CdSeTe/CdS	1 : 2.4	1 : 0.03	0.5:0.5	1:10	11.6	100	20
A4 : CdSeTe/CdS	1 : 2.4	1 : 0.3	0.75:0.25	1:10	11.3	100	40
A5 : CdSeTe/CdS	1 : 2.4	1 : 0.3	0.8:0.2	1:10	11.3	100	40
A6 : CdSeTe/CdS	1 : 4.8	1 : 0.3	0.8:0.2	1:10	11.2	100	40
A7 : CdSeTe/CdS	1 : 3.6	1 : 0.3	0.8:0.2	1:10	11.3	100	40
A8 : CdSeTe/CdS	1 : 3.0	1 : 0.3	0.8:0.2	1:10	11.3	100	40
A9 : CdSeTe/CdS	1 : 1.6	1 : 0.3	0.85:0.15	1:10	11.5	90	40
A10 : CdSeTe/CdS	1 : 0.9 (0.1M Sodium Citrate)	1 : 0.3	0.85:0.15	1:10	11.5	90	40
A11 : CdSeTe-*Core*	1 : 1.6	1 : 0.3	0.85:0.15	*No thiourea*	11.5	90	40
A12 : CdSeTe/CdS	1 : 1.6	1 : 0.3	0.85:0.15	1:10	11.5	90	20
A13 : CdSeTe/CdS	1 : 1.6	1 : 0.3	0.85:0.15	1:10	11.5	90	100

First, $CdCl_2$ / TGA mole ratio was kept constant at 1.0:2.4 and Te:Se mole ratios were changed between 0.9:0.1, 0.85:0.15, 0.8:0.2, 0.75:0.25 and 0.5:0.5, keeping the mole ratio of Cd:(Te+Se) as 1.0:0.3. After determination of the most suitable mole ratio of Se to Te, the mole ratio of $CdCl_2$ to TGA was changed, namely Cd to TGA= 1.0:4.8, 1.0:3.6, 1.0:3.0, 1.0:2.4 and 1.0:1.6. Sodium Citrate (SC) as a co-ligand was also used one time with TGA in the CdSeTe / CdS synthesis. The final concentration of SC was 0.1M. The ratio of S to Se precursor was kept constant as 1.0:10 in all trials.

2.2. Spectroscopic and Microscopic Characterization

Spectral properties of $CdSe_xTe_{1-x}$ and $CdSe_xTe_{1-x}$ / CdS were investigated at room temperature by using Varian Cary 50 UV-Vis Spectrometer and Varian Cary Eclipse Fluorescence Spectrometer. Aliquots taken from flask at different times to monitor particles growth. Nanocrystals have absorption spectra ranging from 480nm to 570nm and their emission spectra changes from 534nm to 610nm.

X-ray powder diffraction (XRD) measurements were done at IYTE-MAM with Philips X-pert Pro Powder Diffractometer with CuKα radiation (λ=1.5406 Å). X-ray source is the Philips high intensity ceramic sealed tube. Data was collected for 2θ values of 20° to 60°. After one step purification with 2-Propanol, precipitated particles were dried at room temperature and then powdered form was used in XRD. The average particle sizes were determined by using recorded with a X'Pert PRO MPD diffractometer (Cu Kγ radiation, with grazing angle 0.5°) in Physics Department at IYTE.

TEM measurements were carried out at UNAM (National Nanotechnology Research Center at Bilkent University in Ankara) to study size distribution, crystal structure and morphology with Tecnai G^2 F30 TEM (FEI). Synthesized nanocrystals was droped on grids for TEM analysis.

Scanning Electron Microscope (SEM) coupled with the energy dispersive x-ray detector (EDX) was used to determine the chemical composition of nanocrystals. Purified nanoparticles was used for the elemental analysis.

Elemental analysis was also carried out by using Agilent 7500ce Inductively Coupled Plasma Mass Spectroscopy (ICP-MS). A calibration curve was established, 1.0 ppm control solution was prepared by Se, Cd and Te standarts and diluted to 750, 500,

250, 100, 50, 20, 10, 5, 2, 1, 0.5, 0.1 and 0.05 ppb, which contain 1 % HNO_3. CdSeTe and CdSeTe/CdS dispersions with 0.1 ppm containing 1 % HNO_3, were analysed.

To study biological responce of nanocrystals of cancer cells (PC3 and MCF7) MTT test was performed. Purified and sterilized nanoparticles were used in MTT test at different concentrations. Results were obtained by taking average of the three replicates for each concentration. It also was repeated for 24, 48 and 72 hours of exposure times. Trypan blue staining was used to to assume cell proliferation. MCF7, A549 and BEAS-2B cell suspensions were used for 24 hours of exposure time in trypan blue cell viability test.

Bioimaging was performed with a confocal microscope (Andor Revolution). During this study, MCF7 cancer cells were used.

1 µg/ml CdSeTe and CdSeTe/CdS nanocrystals in PBS solution were injected into cell medium in 6-well plates, then they were incubated for desired times at 37^0C. The media was aspirated from wells and washed with PBS, then cells was fixed with paraformaldehyde for 10 minutes and fixative solution was aspirated and washed with PBS for 5-10 minutes by shaking. The cells were blocked with 10 % FBS in PBS for 30 minutes with vigorous shaking and washed with PBS three times. After aspiration of the PBS solution, slides were removed from wells and dried. The mounting media was droped onto slide and covered with the dried coverslip, then slides were analysed under confocal microscope with appropriate filters.

CHAPTER 3

PHYSICOCHEMICAL PROPERTIES OF CdSeTe BASED NANOCRYSTALS

3.1. Spectroscopic Properties of $CdSe_xTe_{1-x}$ / CdS Core / Shell Nanocrystals

All absorbance and fluorescence studies were done by taking aliquots from reaction flask at different times. The growth dynamics of nanocrystals can easily be monitored by absorption and fluorescence spectra. The color change of nanocrystals depending on the size, can be observed under UV-lamp.

3.1.1. UV-Vis Absorption and Fluorescence Spectroscopy

Optical properties of synthesized $CdSe_xTe_{1-x}$ / CdS nanocrystals were determined by UV-Vis and fluorescence spectroscopies. In $CdSe_xTe_{1-x}$ / CdS nanocrystal synthesis part of this study, various mole ratios of reactants and reaction conditions were used to optimize spectroscopic properties; e.g. the quantum yield of nanocrystals. In Table 2.1 the reaction parameters were listed for different conditions, each synthesis were coded with a letter A and a number.

In the study of Pan et al. CdSe core was synthesized then it is surrounded with CdS (Pan, et al. 2005). In our work, NaHSe and NaHTe as Se and Te precursors were added to the reaction media at the same time to form alloy structure and then CdS shell was surrounded around $CdSe_xTe_{1-x}$ core, by adding thiourea.

Absorption and emission spectra of synthesized nanoparticles with different compositions are shown respectively, A2 in Figure 3.1, A4 in Figure 3.2, A5 in Figure 3.3, A6, A7, A8 in Figure 3.4, A9 in Figure 3.9 - Figure 3.11, A10 in Figure 3.5, A11 in Figure

3.6, A12 in Figure 3.7, A13 in Figure 3.8. The specimen, which coded as A1 and A3 were give no result so their UV-Vis and emission spectra were not shown.

During the reactions, without any purification aliquots were taken at different times and their UV-Vis and emission spectra were obtained, photoluminescence quantum yield was calculated by Equation (1.2.). Spectral properties, UV-Vis and emission wavelengths, FWHM of emission peaks and calculated photoluminescence quantum yields were listed in Table 3.1. Since we aimed to use these nanocrystals in cellular bioimaging applications, higher photoluminescence quantum yields are important to quantify biological processes in cells.

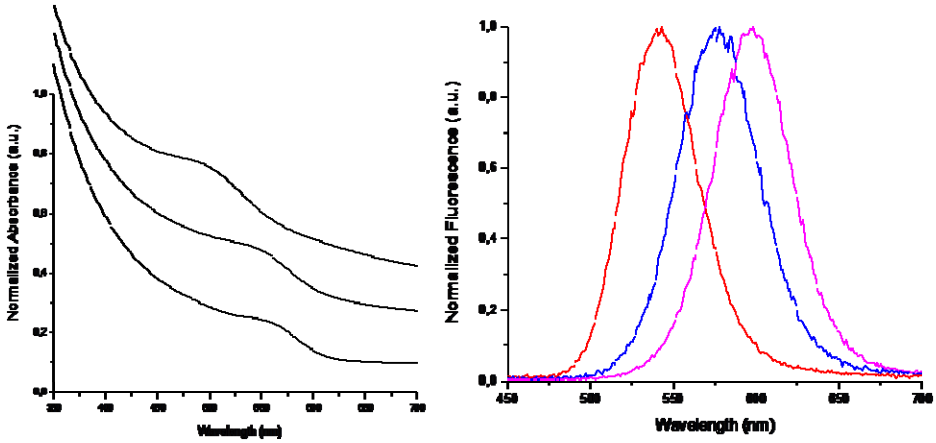

Figure 3.1. UV-Vis and fluorescence spectra of A2-CdSeTe/CdSe nanoparticles.

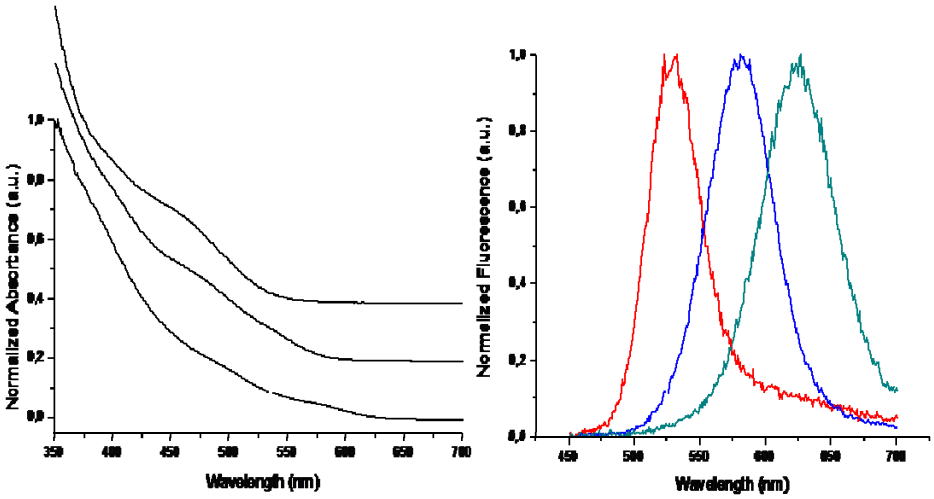

Figure 3.2. UV-Vis and fluorescence spectra of A4-CdSeTe/CdSe nanoparticles.

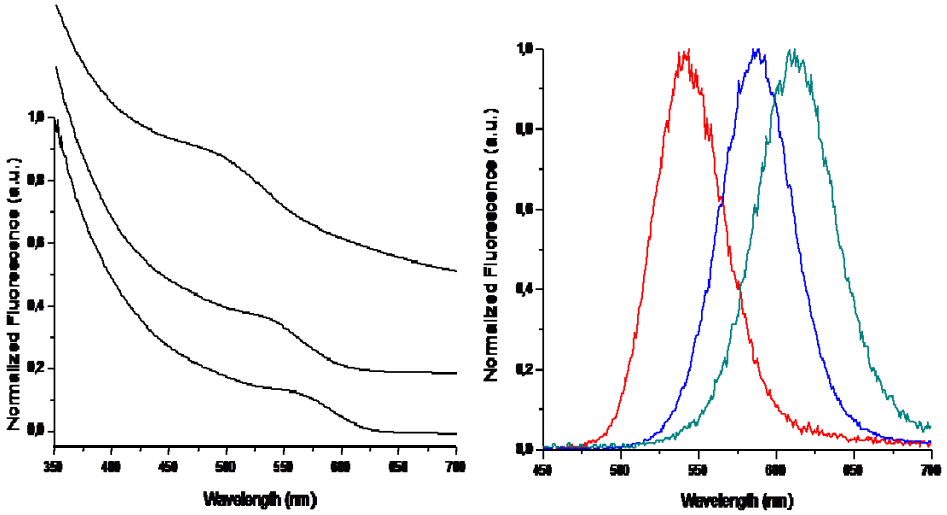

Figure 3.3. UV-Vis and fluorescence spectra of A5-CdSeTe/CdSe nanoparticles.

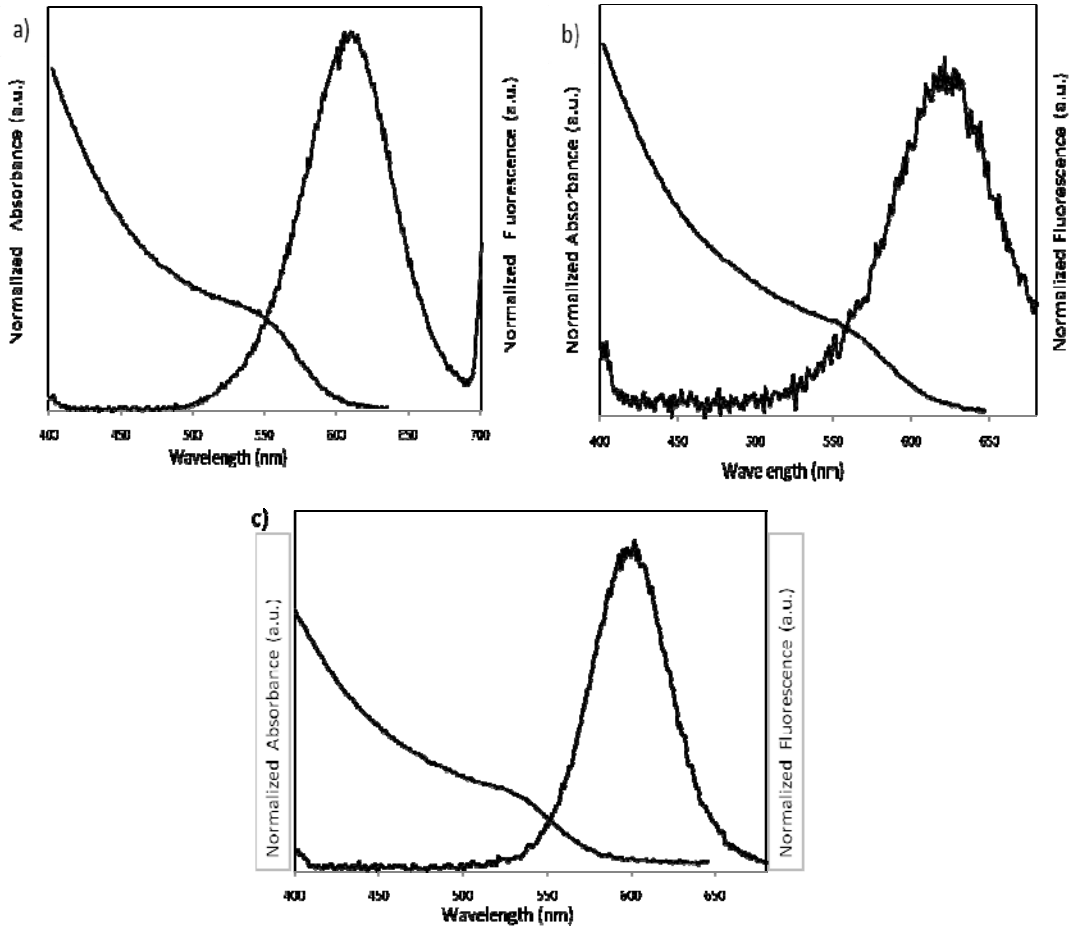

Figure 3.4. UV-Vis and fluorescence spectra of a) A6-CdSeTe/CdSe b) A7-CdSeTe/CdSe c) A8-CdSeTe/CdSe nanoparticles.

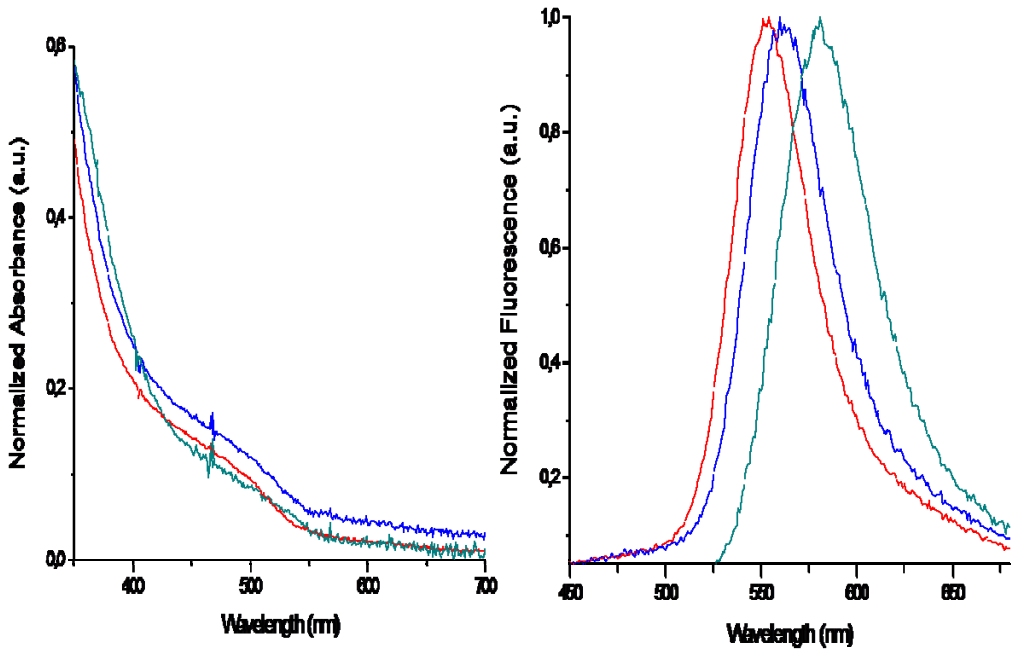

Figure 3.5. UV-Vis and fluorescence spectra of A10-CdSeTe/CdSe nanoparticles.

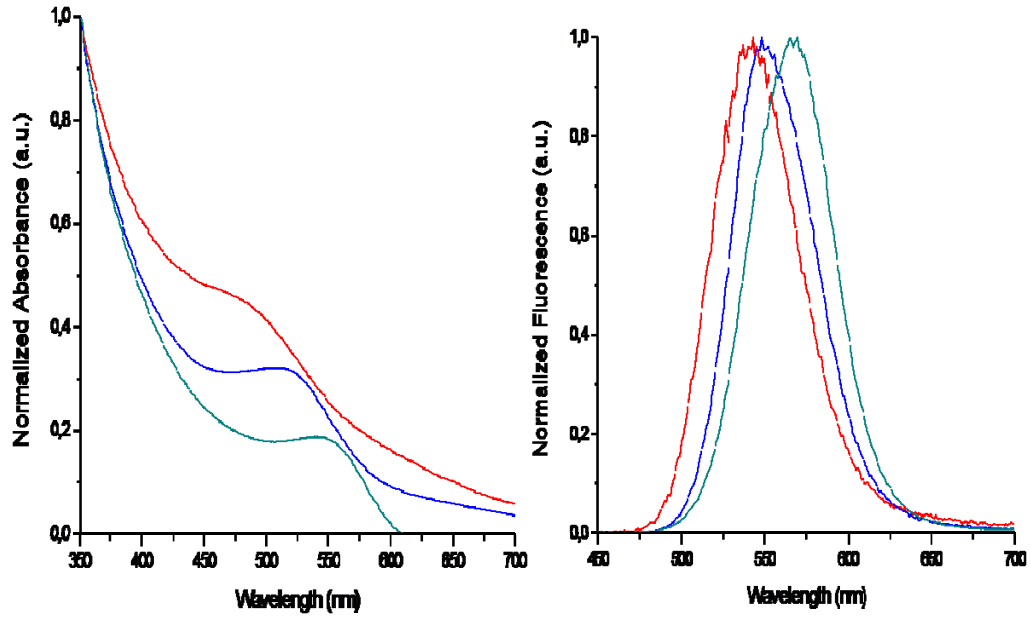

Figure 3.6. UV-Vis and fluorescence spectra of A11-CdSeTe core nanoparticles.

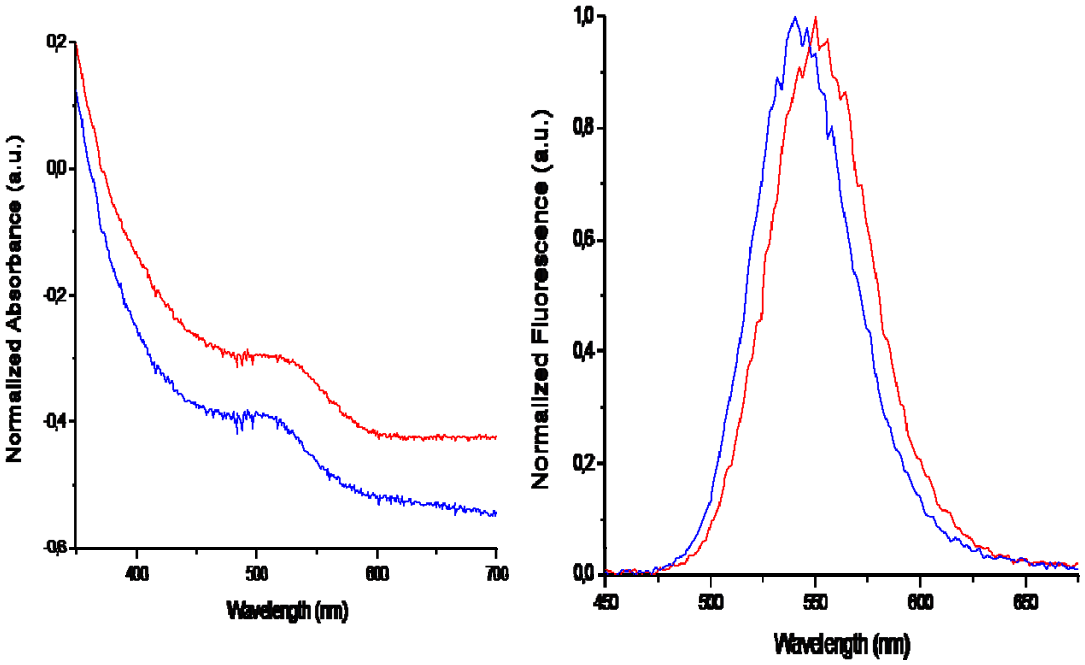

Figure 3.7. UV-Vis and fluorescence spectra of A12-CdSeTe/CdSe nanoparticles.

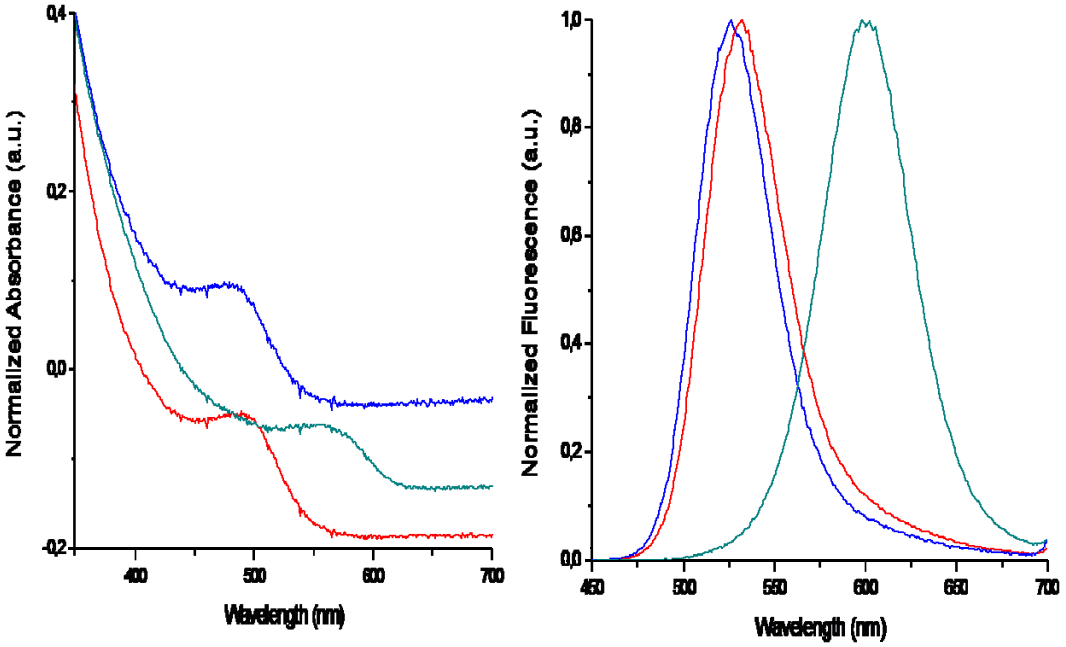

Figure 3.8. UV-Vis and fluorescence spectra of A13-CdSeTe/CdSe nanoparticles.

Table 3.1. Spectral properties of synthesized CdSeTe/CdS nanocrystals.

CODE-	Absorption Wavelength (nm)	Emission Wavelength (nm)	FWHM (nm)	Quantum Yield	Reaction Parameters that is Varying		
					[*Cd:TGA*	[*Cd:(Se+Te)*]	[*Te:Se*]
A1CdSeTe-*Core*	-	-	-	*Not emitting*	1 : 2.4	1:0.3	0.5:0.5
A2 CdSeTe/CdS	555	560	60	7.7%	1 : 2.4	1 : 0.3	0.9:0.1
A3 CdSeTe/CdS	560	655	65	*Not emitting*	1 : 2.4	1 : 0.03	0.5:0.5
A4 CdSeTe/CdS	534	574	55	6.6%	1 : 2.4	1 : 0.3	0.75:0.25
A5 CdSeTe/CdS	552	584	65	8.2%	1 : 2.4	1 : 0.3	0.8:0.2
A6 CdSeTe/CdS	560	603	70	2.1%	1 : 4.8	1 : 0.3	0.8:0.2
A7 CdSeTe/CdS	563	606	90	0.5%	1 : 3.6	1 : 0.3	0.8:0.2
A8 CdSeTe/CdS	556	602	55	0.2%	1 : 3.0	1 : 0.3	0.8:0.2
A9 CdSeTe/CdS	516	551	50	22.2%	1 : 1.6	1 : 0.3	0.85:0.15
A10CdSeTe/CdS *TGA-SC capped*	495	553	52	5.6%	1 : 0.9 (0.1M Sodium Citrate)	1 : 0.3	0.85:0.15
A11 CdSeTe	485	535	55	17.3%	1 : 1.6	1 : 0.3	0.85:0.15
A12CdSeTe/CdS	502	540	55	7.5%	1 : 1.6	1 : 0.3	0.85:0.15
A13CdSeTe/CdS	506	598	50	11%	1 : 1.6	1 : 0.3	0.85:0.15

These systematic studies led to the optimization of synthetic parameters for preparing CdSeTe/CdS nanocrystals with high quantum yield and with narrow FWHM. The optimum reaction conditions and molar ratios were determined based on the highest photoluminescence quantum yield of the nanocrystals. The best sample is A9; its quantum yield was 22, 2% and FWHM of emission spectrum of A9 was 50nm.

In our study, the FWHM of emission spectra of different samples, from A2 to A13, varied from 50nm to 90nm. In Piven et.al.'s study, FWHM of CdSeTe / CdS

nanoparticles varied from 42 nm to 110 nm by changing the Se/ Te ratio in alloy composition. In their study, they obtained larger FWHM as increasing the Se ratio (Piven, et al. 2008). In our study FWHM were not change with Se/Te mole ratio. Increase in FWHM may be due to polydispersity of CdSeTe / CdS nanoparticles or may cause from the decreasing crystalline quality of samples.

As the number of defect states is decreased, nanoparticles should have better crystal structure and as a result, the photoluminescence quantum yields of the nanoparticles should increase. In literature, Jiang et al. mentioned that alloyed CdSeTe nanocrystals synthesized by organometallic route have quantum yield around 30% which is considered as to be high (Jiang, et al. 2006). Even we synthesis the particles in aqueous medium, we get 22% of quantum yield that produces a higher brightness (a measure of observing emitting scale of materials) for cellular imaging applications.

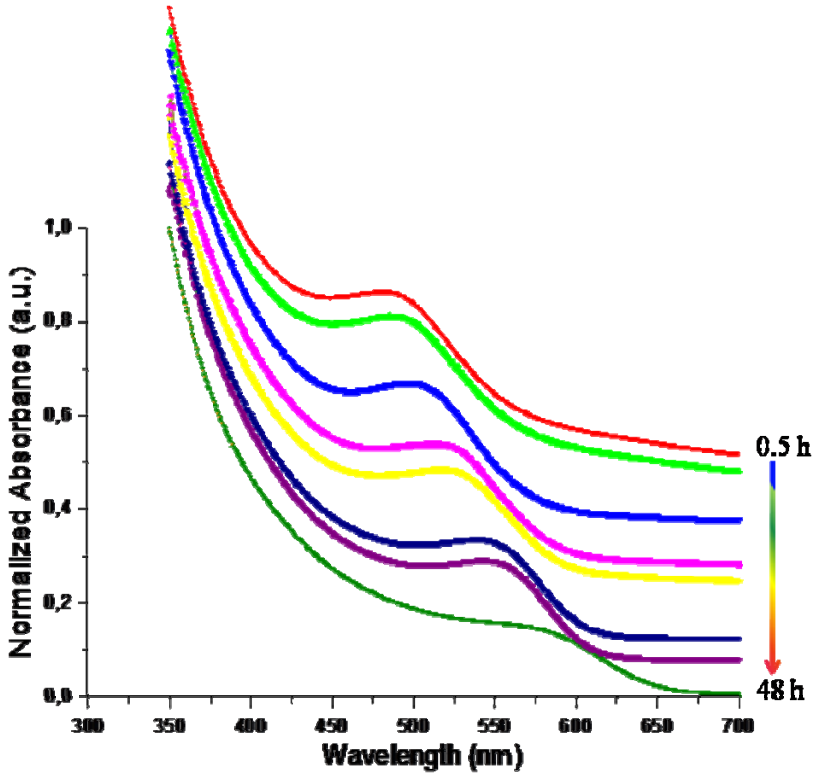

Figure 3.9. Normalized UV-Vis spectra of A9 – CdSeTe / CdS nanoparticles, aliquots taken at different times.

The growth of CdSeTe/CdS nanoparticles can be observed by using UV-Vis spectroscopy (Figure 3.9). A steady shift of spectra to higher wavelengths is obvious; indicating an increase in the size of CdSeTe / CdS nanoparticles.

Nanocrystals can be continuously excited in a range from 350nm to 600nm which is an advantageous in labeling applications.

In this study, green, yellow and orange colors were clearly observed due to change in the size of CdSeTe / CdS nanoparticles. The color change of CdSeTe / CdS nanoparticles under day light and under UV-lamp can be seen in Figure 3.10. Color change in CdSeTe / CdS observed in this work was convenient with literature (Rogach, et al. 2007, Gaponik, et al. 2002, Peng, et al. 2007). The color of the CdSeTe / CdS nanoparticles can be tuned by time from green to orange because the conduction and valance band in quantum dots get closer when quantum dots are larger. The band gaps of particles are decreased as the particle size increased (Table 3.2.).

a) b)

Figure 3.10. Images of CdSeTe / CdS nanoparticles, a) under day light b) under UV lamp.

Emission spectra show time dependent growth of CdSeTe / CdS nanoparticles. During the growth of CdSeTe / CdS nanoparticles, the spectra shift to higher wavelengths (Figure 3.11). At the beginning of the reaction, nanocrystals emit at 534nm and after 48 hours, the emission wavelength reaches to 610nm. As the size of particles increase, as a consequence of quantum confinement effect red shifted emission spectra were obtained. The fluorescence spectra of the nanocrystals show a symmetrical shape with a spectral width (FWHM) of around 50 nm.

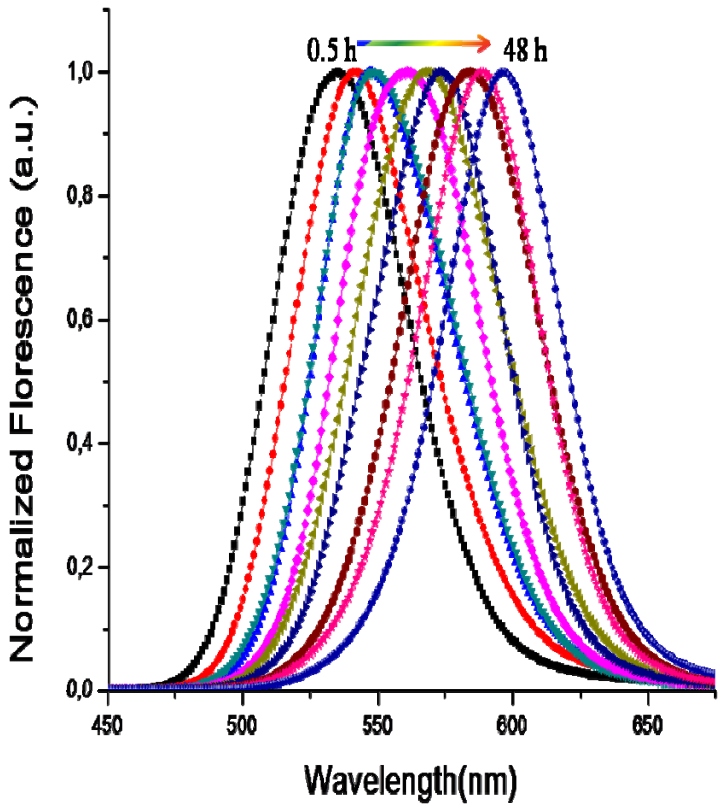

Figure 3.11. Normalized fluorescence spectrum of A9 - CdSeTe / CdS nanoparticles, aliquots was taken at different time intervals.

Quantum yields (QY) of the nanoparticles were calculated by using Rhodamine 6G in water (QY: 95%) as reference. QY of A9 CdSeTe/CdS nanoparticles varied between 8% and 22%, the highest QY was observed from emission spectra at 550nm when the color was yellow. At the beginning of the reaction (emission wavelength at 534nm), alloy CdSeTe nanocrystals' QY was 12% but after CdS shell coating, QY of CdSeTe/CdS nanocrystals increased to 22%. This increase in QY was followed by a decrease around 8% (emission wavelength at 600 nm).

When the size of nanocrystals becomes closer to bulk, quantum yield decreases and the changes depend on crystal structure of nanocrystals (Zhong, et al. 2008). At the beginning of the reaction, during the formation of nanocrystals, crystal structure is not perfectly orderred, so QY is low. Within increase in reaction time, nanocrystals are larger in size and better in crystal structure with less surface defects, and then QY is increased. However, when nanocrystals are close to bulk structure, around red color,

this time the surface of nanocrystals start to deform and structural defects form, nanocrystals tend to agglomerate, and QY decreases

In Figure 3.12, the growth of CdSeTe / CdS nanoparticles is shown. At the beginning of the reaction, particle growth was quick but when the particle size increased, the growth slowed down. As the size of particles increases, capping agent might need more time to cover the surface of particles and because the total surface area of all QDs increases the initial growth rate is high. The gradual decrease in growth rate could be caused by a decrease in the concentration of monomers that are consumed during the reaction or larger particles might have more surface defect with respect to smaller ones.

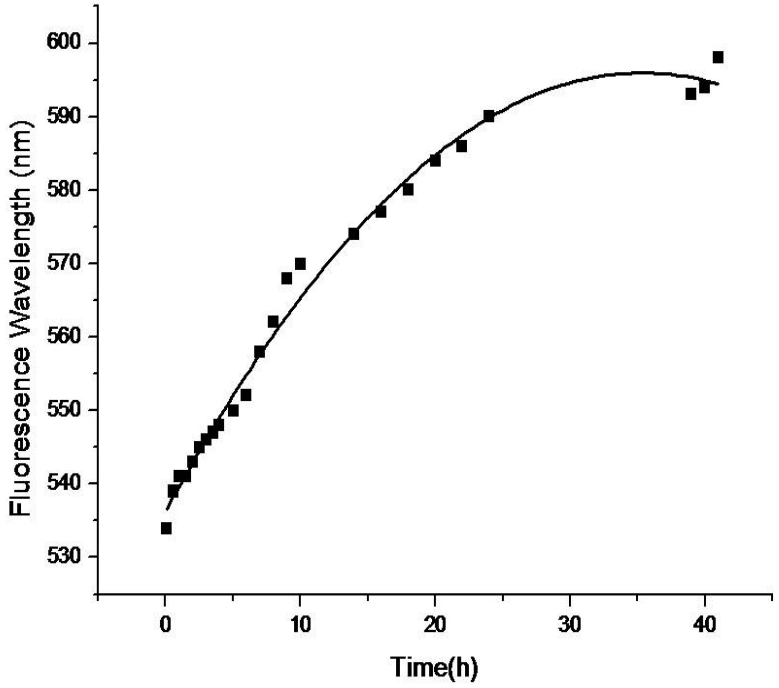

Figure 3.12. Temporal evolution of fluorescence peaks of CdSeTe / CdS nanoparticles.

Table 3.2 Photophysical Parameters of CdSeTe / CdS nanoparticles (A9)

Sample Name - Growth Time (h)	Absorbance Wavelength (nm)	Emission Wavelength (nm)	Quantum Yield (%)	Stokes Shift (nm)	FWHM (nm)	Bandgap (eV)
A9 CdSeTe - 1	480	534	12	46	45	2,24
A9 CdSeTe/CdS - 1,5	500	547	16	53	50	2,18
A9 CdSeTe/CdS - 2,5	515	550	22	65	50	2,14
A9 CdSeTe/CdS - 16	540	583	13	43	60	2,03
A9 CdSeTe/CdS - 45	570	600	8	30	60	1,96

3.2. Structural Characterization

Structural characterization of semiconductor nanoparticles can be conducted by X-Ray Diffractometer (XRD) and Transmission Electron Microscopy (TEM).

3.2.1. X – Ray Diffractometer (XRD)

XRD is used to estimate the crystal structure of $CdSe_xTe_{1-x}$ core and $CdSe_xTe_{1-x}$ / CdS core/shell nanoparticles and also it is used to calculate average crystalline size.

By comparing CdS and CdTe bulk structures hkl indices, $CdSe_xTe_{1-x}$ nanoparticles crystal structure was estimated to be face centered cubic. The diffraction pattern closely matches with a zinc blend structure model. XRD results are convenient with the literature. (Rogach, et al. 2007, Piven, et al. 2007, Deng, et al. 2006).

For comparison the powder patterns which correspond to the (111), (220), and (311) planes of zinc-blende phase for cubic CdS and CdTe are shown in the black and red lines, respectively in Figure 3.13. The X-ray diffraction patterns of nanocrystals

coated with CdS show a strong influence of the CdS shell on the overall diffraction patterns.

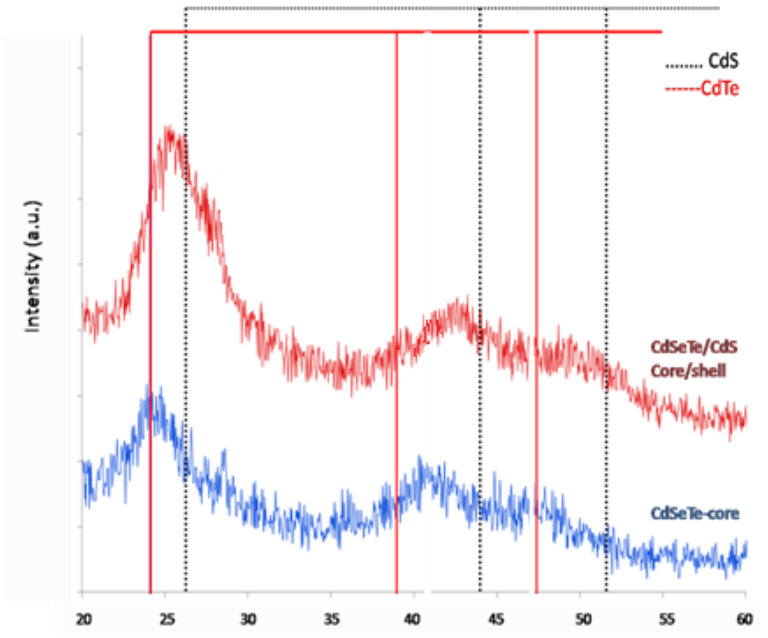

Figure 3.13. XRD spectra of core CdSeTe alloy nanoparticles (red), core /shell CdSeTe/CdS nanoparticles (blue).

Standard patterns of CdS and CdTe are found from literature, Pons, et al. 2009, which are shown in Figure 3.13. XRD peaks of nanoparticles are located between CdTe and CdS phase. From Figure 3.13 CdS shell formation around CdSeTe core can be estimated, in Core / shell nanoparticles' XRD pattern there is a shift through the CdS location.

Core / shell structure of CdSeTe / CdS nanoparticles can be estimated by XRD studies. If nanoparticles are composed of only core CdSeTe, the XRD peaks should not shift to the higher diffraction angles, they should remain unshifted. The shift of nanoparticles to the larger angles points out that CdS shell grows around CdSeTe core. The shift in XRD pattern after thiourea addition for CdS shell formation can be seen in our work. The results agree with literature, (Figure 1.8 , Pons, et al. 2009).

Average crystallite sizes of A11-$CdSe_xTe_{1-x}$ core and A9-$CdSe_xTe_{1-x}$/CdS core/shell nanoparticles were determined from XRD patterns, as illustrated in Figure 3.15, by applying FWHM to the most intense peak using Debye Scherrer equation, (Equation (1.4)). Determined particle size of core A11-CdSeTe and core/shell A9-CdSeTe/CdS nanoparticles are 3.7nm and 4.6nm, respectively.

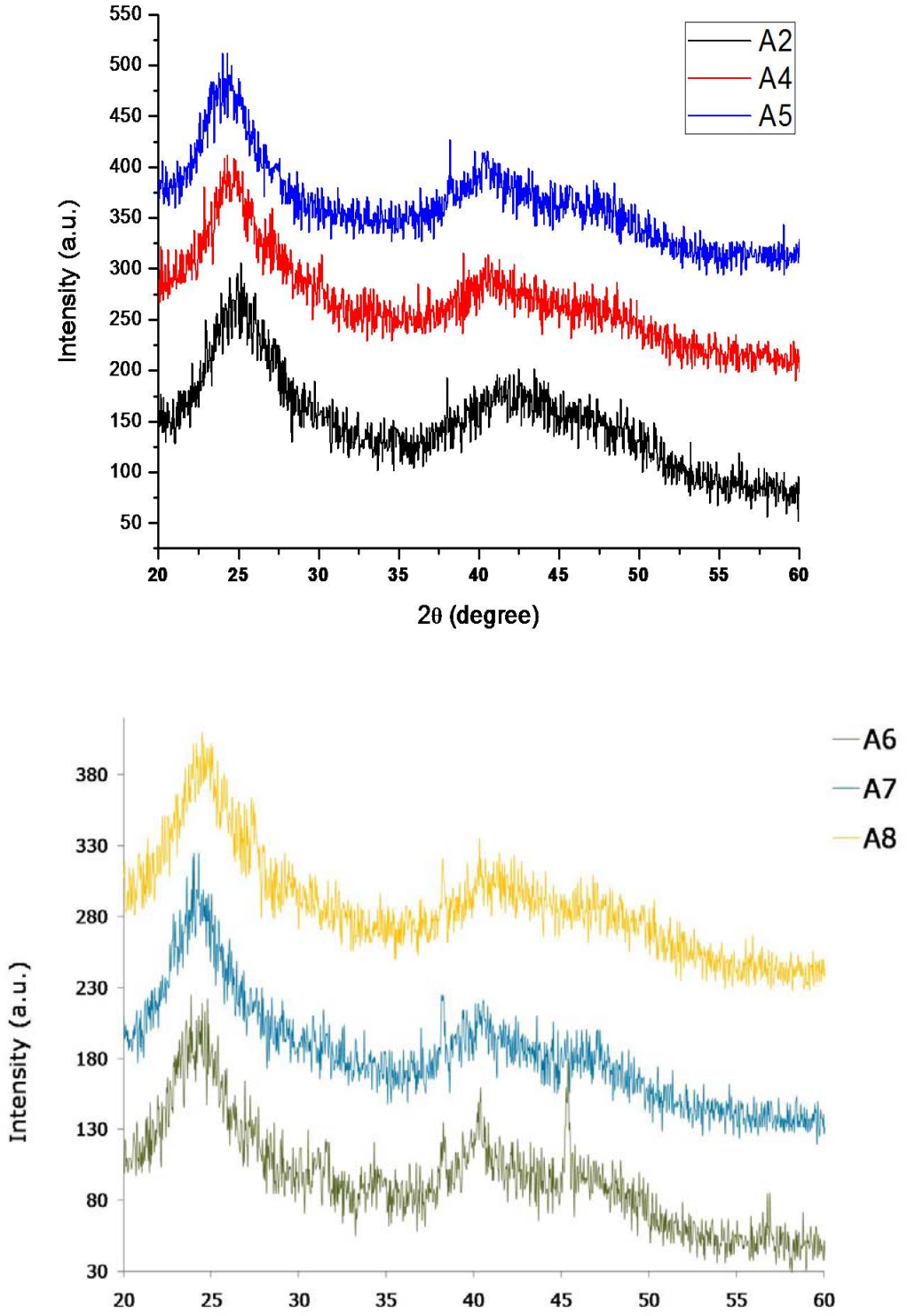

Figure 3.14. XRD patterns of CdSeTe/CdS nanoparticles with different compositions (Table 2.1).

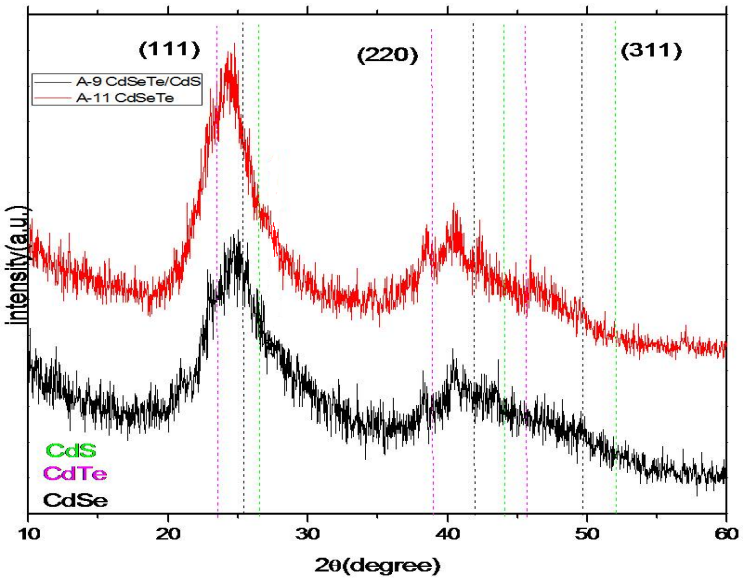

Figure 3.15. XRD pattern of synthesized A9-CdSeTe/CdS core/shell (black) and A11-CdSeTe core (red) nanocrystals .

Compositions of A2, A4, A5, A9 and A11 nanoparticles were determined from XRD patterns, as illustrated in Figure 3.14 and Figure 3.15 by applying Vegard's law to most intense (111) peaks (Equation (1.9)). At the beginning of reactions different mole ratios of Se and Te precursors were used (Table 2.1). Determined alloy compositions are listed in Table 3.3.

Table 3.3. Compositions of nanoparticles contain different amounts of Se and Te precursors

Code	Te:Se Mole Ratio	Composition from Vegard's Law
A2-$CdSe_xTe_{1-x}$/CdS	0.9 : 0.1	$CdSe_{0,792}Te_{0,208}$
A4-$CdSe_xTe_{1-x}$/CdS	0.75 : 0.25	$CdSe_{0,437}Te_{0,563}$
A5-$CdSe_xTe_{1-x}$/CdS	0.8 : 0.2	$CdSe_{0,271}Te_{0,729}$
A9-$CdSe_xTe_{1-x}$/CdS	0.85 : 0.15	$CdSe_{0,635}Te_{0,365}$
A11-$CdSe_xTe_{1-x}$	0.85 : 0.15	$CdSe_{0,315}Te_{0,685}$

Crystallite size calculations were done for A13-CdSeTe/CdS nanocrystals with aliquots taken from reaction flask at different times by applying FWHM of the most

intense peak to Debye–Scherrer equation(Equation (1.4)) and listed in Table 3.4. Average crystallite sizes were determined from XRD patterns, illustrated in Figure 3.16.

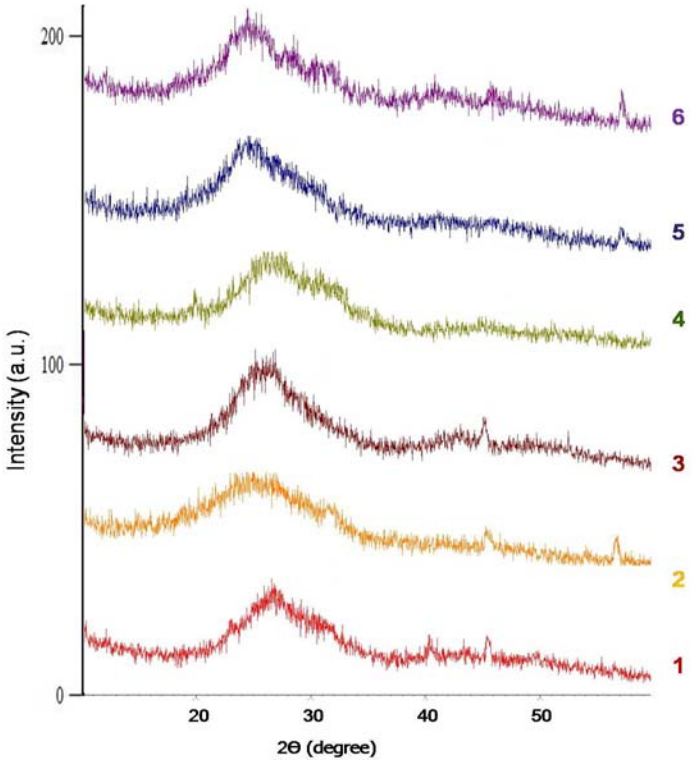

Figure 3.16. XRD spectra of A13 CdSeTe / CdS nanoparticles, aliquots were taken at different times.

Table 3.4 Photophysical and Structural Properties of CdSeTe / CdS nanoparticles

Name	Absorbance Wavelength (nm)	Emission Wavelength (nm)	Absorbance Onset (nm)	Bandgap (eV)	Size From XRD (nm)
1-CdSeTe/CdS	497	545	576	2.15	1.7
2-CdSeTe/CdS	518	568	600	2.06	1.9
3-CdSeTe/CdS	536	577	605	2.04	2.1
4-CdSeTe/CdS	540	590	611	2.03	2.3
5-CdSeTe/CdS	555	598	623	1.99	2.7
6-CdSeTe/CdS	565	600	658	1.98	3.2

3.2.2. Transmission Electron Microscopy (TEM)

TEM images provide information about size and morphology of nanoparticles. TEM grids were prepared by dropping diluted dispersions of CdSeTe/CdS nanocrystals to observe size and structures of the nanocrystals. The particle size for sample A10 is determined to be 5.0 nm. The particles indicate almost same monodispersity (Figure 3.17). A crystalline structure can be seen from the TEM images which indicate crystal formation at nanometer scale.

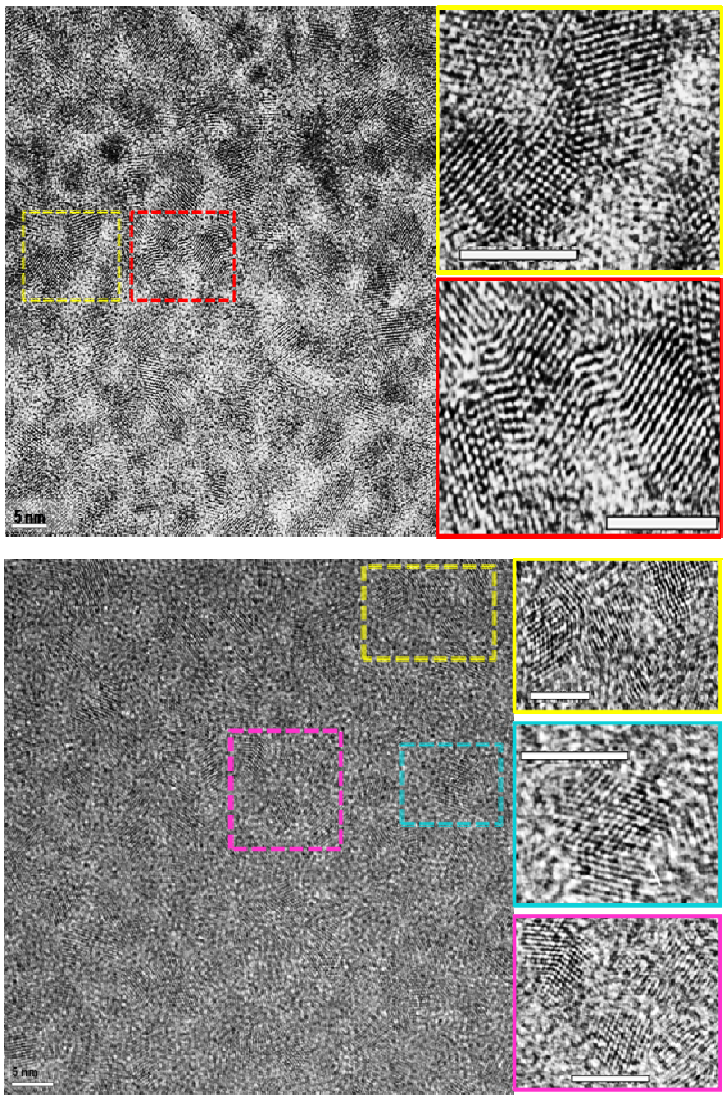

Figure 3.17. TEM images of CdSeTe/CdS core/shell nanoparticles. (Scales are 5nm).

Information about distribution of Se and Te in nanoparticles was also investigated by energy filtered TEM images. In Figure 3.18. (a) shows Se mapping and (b) shows the Te mapping. We can conclude that almost all nanocrystals contain both Se and Te.

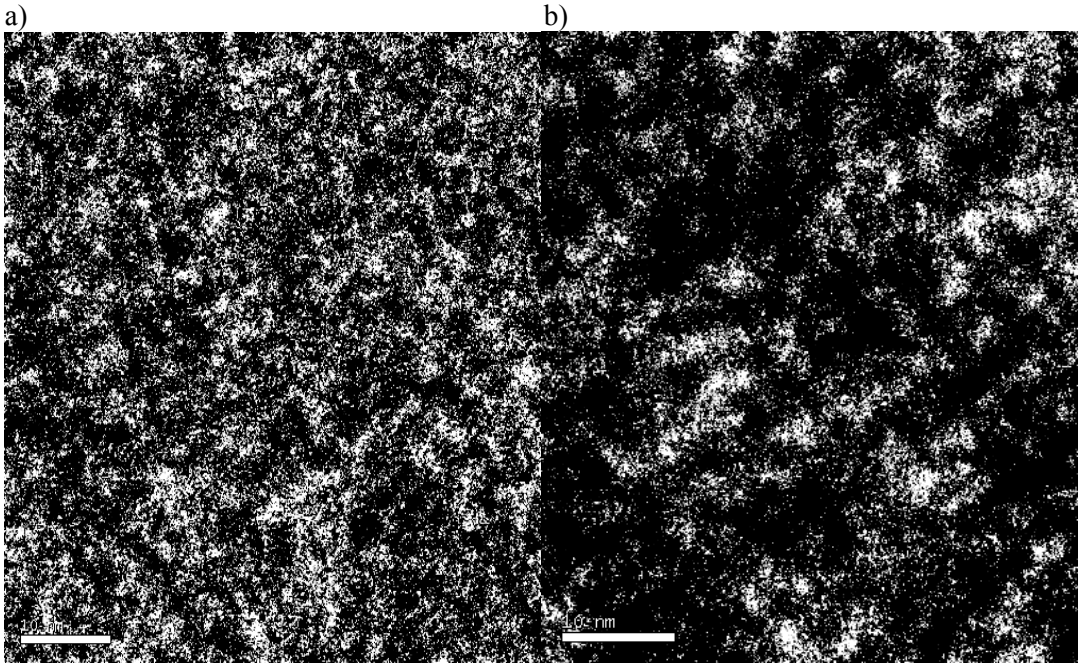

Figure 3.18. EF-TEM images of CdSeTe / CdS core/shell nanoparticles shows a) selenium and b) tellerium mapping (Scales are 10nm).

3.3. Elemental Analysis

Elemental analysis was carried out by using Agilent 7500ce Inductively Coupled Plasma Mass Spectroscopy (ICP-MS). All samples were dissolved in aqueous solution 1% HNO_3. The $CdSe_xTe_{1-x}$ and $CdSe_xTe_{1-x}$ / CdS nanoparticles are prepared with 0.1 ppm concentration ns. Concentration of Cd, Te and Se are shown in Table 3.5. Mole ratios of Cd to (Se+Te) was 1:0.3 and Se:Te was 1.5:8.5 at the beginning of reaction. ICP-MS analysis showed that both $CdSe_xTe_{1-x}$ core and $CdSe_xTe_{1-x}$ / CdS core/shell nanoparticles contain trace amount of selenium compared to amount of Cd and Te (Table 3.5). This is an expected result since very small amount of Se was injected to reaction media during synthesis.

Table 3.5. ICP-MS results of core and core/shell nanoparticles.

Sample	Se (ppb)	Te (ppb)	Cd (ppb)	Se:Te	Cd/(Se+Te)
CdSeTe Core	26	218	755	0.19	3.29
CdSeTe/CdS Core/Shell	6	226	669	0.04	3.22

Scanning Electron Microscope (SEM) Energy dispersive x-ray (EDX) spectrum were also used for elemental analysis. Qualitative determination of A9-CdSeTe/CdS core and A11-CdSeTe/CdS core/shell nanocrystals were done by EDX analysis, which is illustrated in Figure 3.19 Cd, Se, Te and S elements were present in the analysed area.

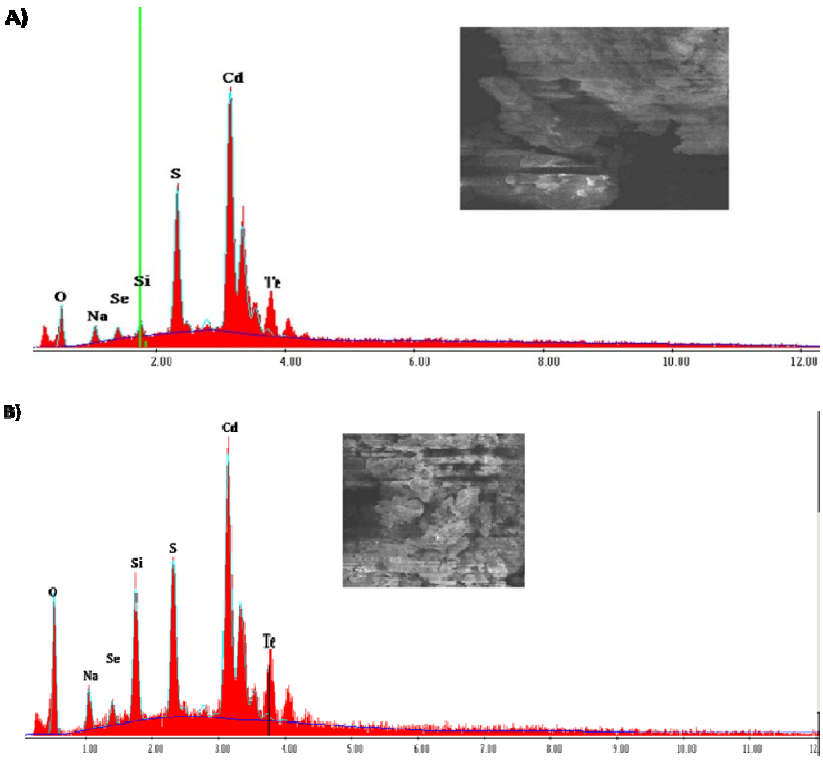

Figure 3.19. EDX analysis a) CdSeTe/CdS core/shell and b) CdSeTe core nanocrystals. SEM images are provided for the area analysed by EDX.

CHAPTER 4

EVALUATING BIOLOGICAL RESPONSE OF HUMAN CELLS TO CdSeTe NANOPARTICLES

In this chapter biological response of human prostate cancer cells (PC3) and breast cancer cells (MCF7) to CdSeTe / CdS nanocrystals are evaluated by MTT test and confocal microscopy.

Carcinomic human alveolar basal epithelial cells (A549), human bronchial epithelial cells (BEAS-2B) were used to evaluate cell membrane integrity and thus assume cell proliferation by trypan blue staining.

4.1. MTT Studies

To understand the cytotoxic activity of synthesized nanoparticles MTT assay was performed for identification of proliferation the cell populations. The determination of cell growth was done by counting viable cells after staining with a yellow MTT (3-(4,5-Dimethylthiazol-2-yl)-2,5-diphenyltetrazolium bromide) which was reduced to purple formazan in the mitochondria of living cells. Human Prostate Cancer (PC3) cell line and breast cancer (MCF7) cell line were used during this process.

PC3 cell line was kindly provided by Associate Professor Kemal Sami Korkmaz (Ege University, Engineering Faculty, Department of Bioengineering), MCF7 cell line was obtained from Professor Neşe Atabey (Dokuz Eylül University, Medical School, Department of Medical Biotechnology and Genetics). PC3 cells were maintained in Dulbecco's modified Eagle's medium (DMEM) containing 5% fetal bovine serum (FBS), 100µg/mL streptomycin/100IU/mL penicillin. MCF7 cell line was maintained in Roswell Park Memorial Institude-1640 (RPMI-1640) containing 15% FBS (BIO-IND), 100µg/mL streptomycin/100IU/ml penicillin incubated at 37^0C in the dark with 5% CO_2

humidified incubator. The cells were passaged when they reached 80-85% confluency. Cells used in experiments were maintained up to 20^{th} passages.

At the beginning of MTT protocol, the stock solution (5mg/ml) in PBS was prepared and sterilized by using filter, it should be stored at 4^0C (solution is stable ~ 6 weeks). MTT stock solution can be used by adding 1:10 ratio into wells (directly from stock for suspension cells). Wells should be covered with foil to avoid exposure of direct light.

The nanoparticles were added in 96-well microculture plates, at 1x104 cells density per well, while the final concentration were; 0.0001µg/ml, 0.001µg/ml, 0.01µg/ml, 0.1µg/ml, 1µg/m, l2.5µg/ml, 5µg/ml, 10µg/ml, 25µg/ml, 50µg/ml, 100µg/ml for both A9-CdSeTe / CdS nanoparticles and A10–CdSeTe / CdS nanoparticles. Each measurement was repeated 3 times (triplicate). Cells were treated with the nanoparticles for 24, 48 and 72 hours, and cytotoxic effects were determined by tetrazolium based colorimetric assay. Briefly; 4 hours before the end of each incubation period, medium of the cells was removed and wells were washed by pre-warmed phosphate-buffered saline (PBS) to remove any trace of the nanoparticles and to prevent color interference while optical density determination. MTT stock solution (5mg/ml) was diluted at 1:10 ratio into complete culture media, 100µl of MTT dilution was added into each well and incubated. After 3.5 hours, the plates were centrifuged at 1800 rpm for 10 minute at room temperatures and then supernatant was removed by tapping. Mitochondrial dehydrogenases of viable cells cleave the tetrazolium ring, yielding purple MTT formazan crystals which are insoluble in aqueous solutions. Formazan crystals were dissolved with 100µl DMSO by shaking the wells at 150 rpm for 5min. The resulting purple solution was spectrophotometrically measured. An increase in cell number results in an increase in the amount of MTT formazan formed and an increase in absorbance. The absorbance was determined at 540nm. Results were represented as percentage viability and calculated by the following formula:

$$\% \text{ viability}=100-[(OD_s-OD_b/OD_c-OD_b)x\ 100] \quad (4.1)$$

where OD_b,OD_s, and OD_c indicate the optical density of blank, sample and control respectively.

Lethal concentrations were measured by determining the concentration of A9-CdSeTe / CdS nanoparticles (Figure 4.1 and Figure 4.2) and A10-CdSeTe / CdS

nanoparticles (Figure 4.3 and Figure 4.4). The relative error bars were shown for each 24h, 48h and 72h incubation periods. Each measurement was repeated 3 times (triplicate).

For A9-CdSeTe/CdS nanoparticles, the lethal concentration of free cadmium ions, Cd^{+2}, which cause damage in mitochondria and oxidative stress in cells, was observed above the concentration of 1μg/ml for PC3 cell lines. We observed that synthesized nanoparticles have no significant toxic effect on PC3 cells below the concentration range of 0.1μg/mL (Figure 4.1). Nanoparticles show toxic effects depending on concentration and also incubation period. For 48 hours and 72 hours 2.5μg/mL and above concentrations showed cell viability around 1%, on the other hand for 24 hours at the same concentrations cell viability gradually decreased.

On the other hand, A9-CdSeTe / CdS nanoparticles showed less toxic effects for MCF7 cells than PC3 cells. The lethal concentration of free cadmium ions, Cd^{+2}, was observed above the concentration of 10μg/ml for MCF7 cells (Figure 4.2).

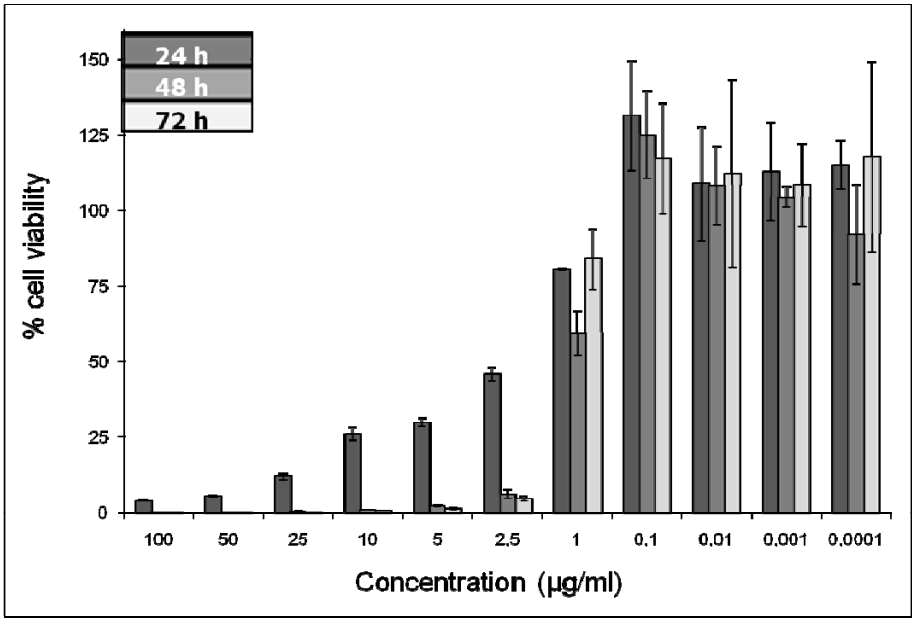

Figure 4.1. MTT results for A9-CdSeTe / CdS quantum dots in PC3 cells for 24h, 48h and 72h treatment (size of nanocrystal determined by XRD as 4.6nm, emitting at 600nm).

For A10-CdSeTe/CdS nanoparticles, the lethal concentration of free cadmium ions, Cd^{+2}, was observed above the concentration of 1μg/ml for PC3 cells (Figure 4.3). A10-CdSeTe/CdS nanoparticles have no any significant toxic effect on PC3 cells below

the concentration 0.1µg/mL. The lethal concentration of free cadmium ions, Cd^{+2}, was observed above the concentration of 25µg/ml MCF7 cells (Figure 4.4).

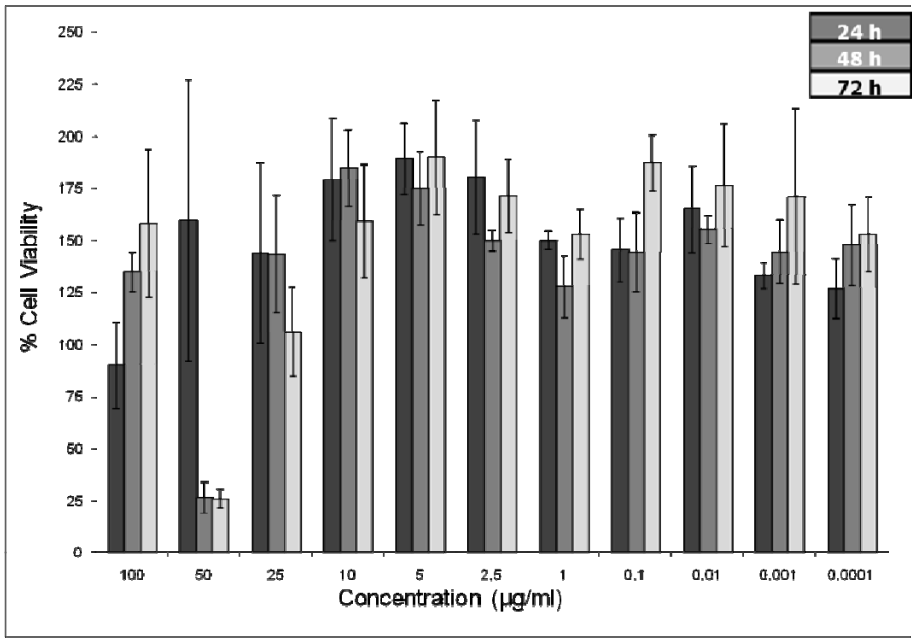

Figure 4.2. MTT results for A9-CdSeTe/CdS quantum dots in MCF7 cells for 24h, 48h and 72h treatment (size of nanocrystal determined by XRD as 4.6nm, emitting at 600nm).

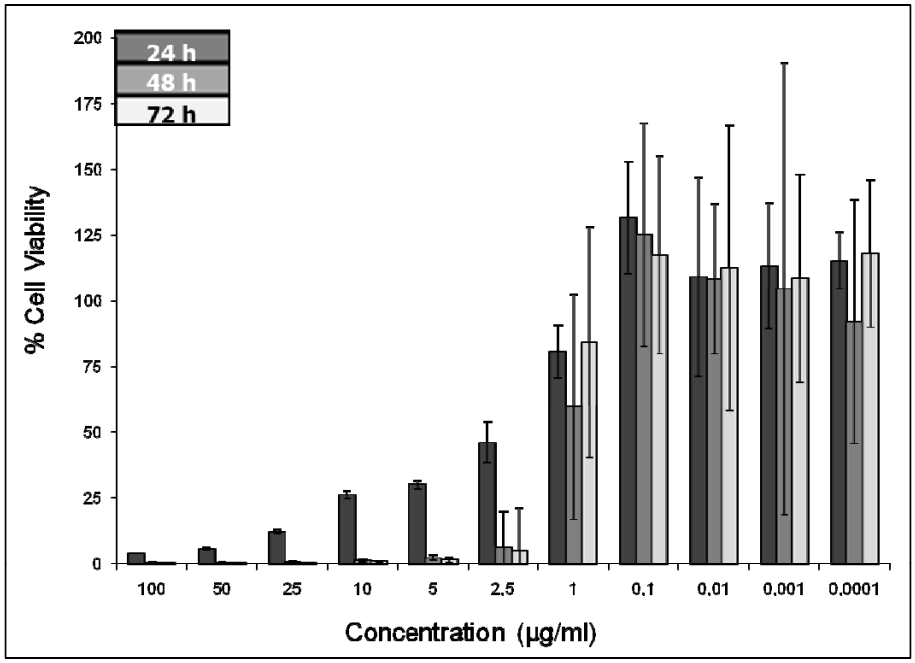

Figure 4.3. MTT results for A10-CdSeTe / CdS quantum dots in PC3cells for 24h, 48h and 72h treatment (size of nanocrystal determined by TEM as 5.5nm, emitting at 580nm).

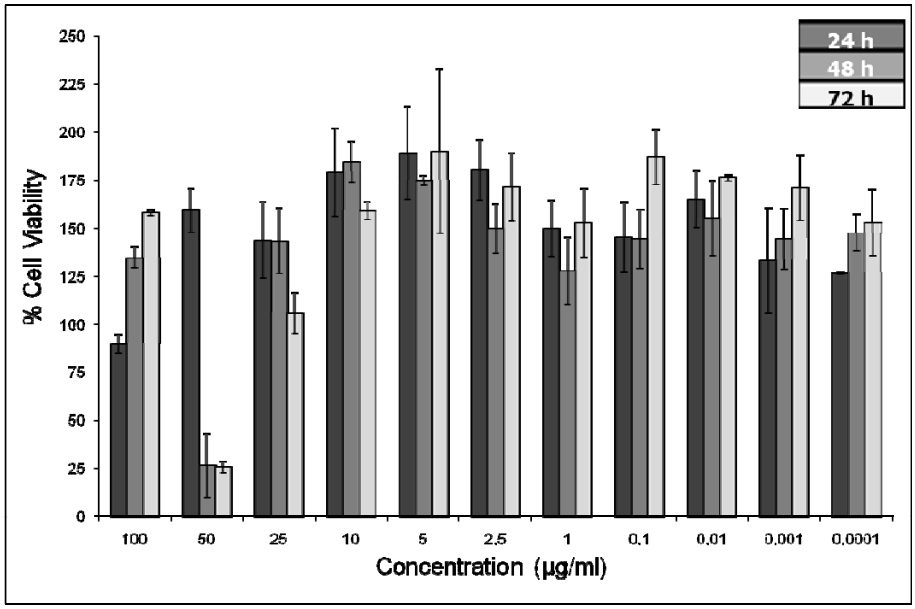

Figure 4.4. MTT results for A10-CdSeTe/CdS quantum dots in MCF7cells for 24h, 48h and 72h treatment (size of nanocrystal determined by TEM as 5.5nm, emitting at 580nm).

MTT test was carried out to be incubated with PC3 and MCF7 cells with $CdCl_2$ and thiourea for 24 hours, $CdCl_2$ was used as free Cd^{+2} source. Lethal concentration of Cd^{2+} ions was 25.0µg/ml for MC7 cells and 1.0µg/ml for PC3 cells (Figure 4.5, Figure 4.6)

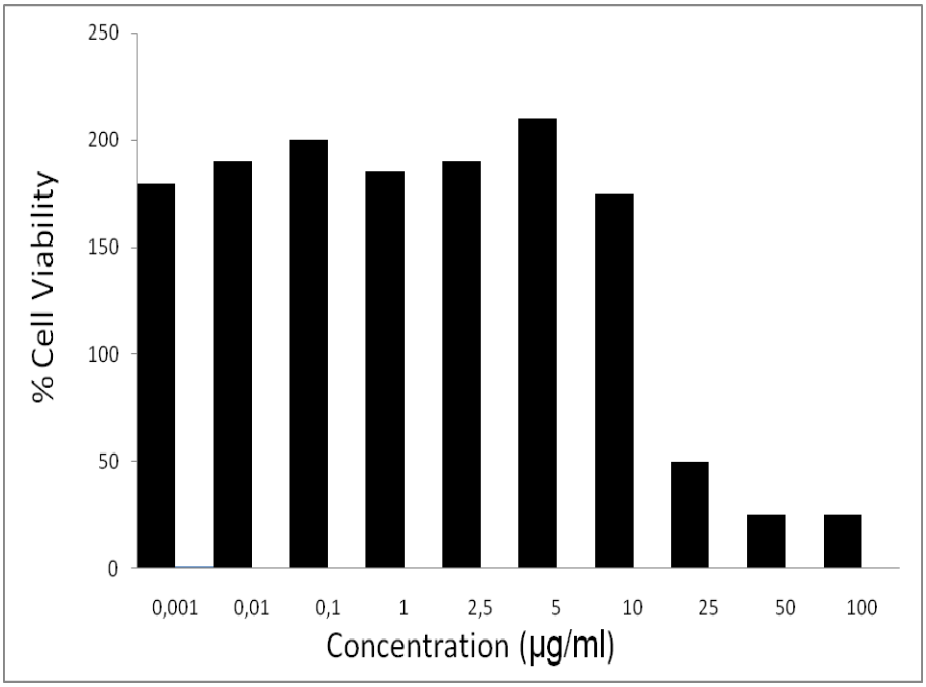

Figure 4.5. MTT results for $CdCl_2$ in MCF7 cells for 1 day.

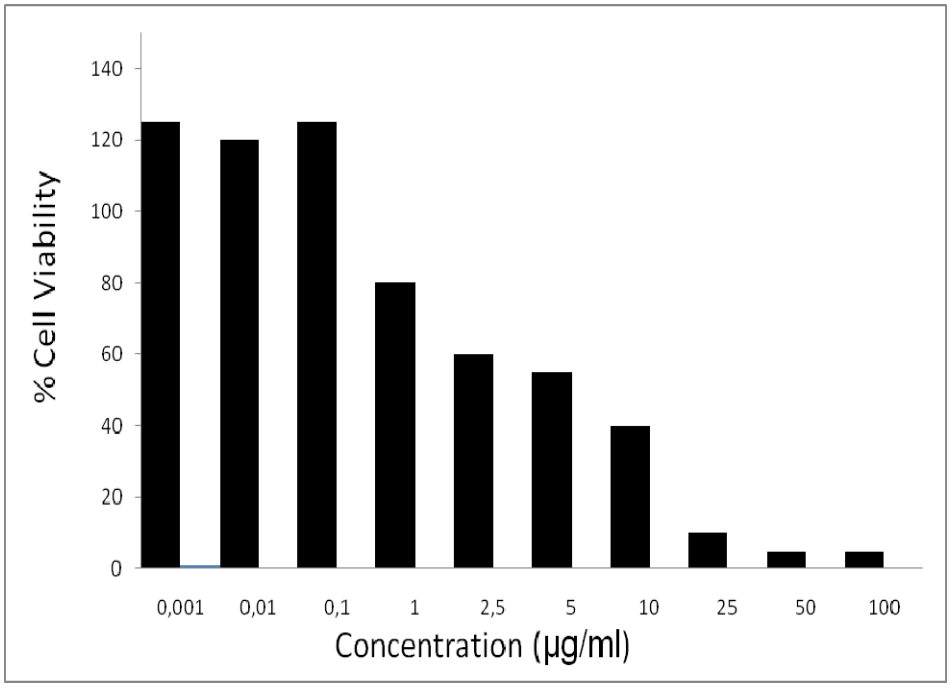

Figure 4.6. MTT results for $CdCl_2$ in PC3 cells for 1 day.

As S-source, thiourea was used and it was observed that thiourea is not toxic for MCF7 and PC3 cells (Figure 4.7, Figure 4.8) for given concentrations.

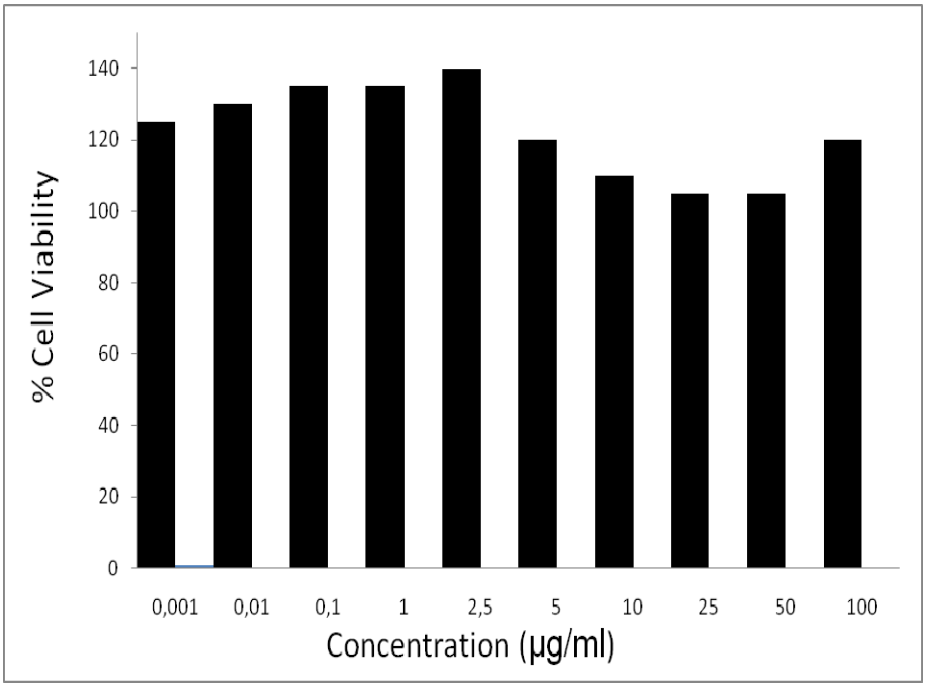

Figure 4.7. MTT results for thiourea in MCF7 cells for 1 day.

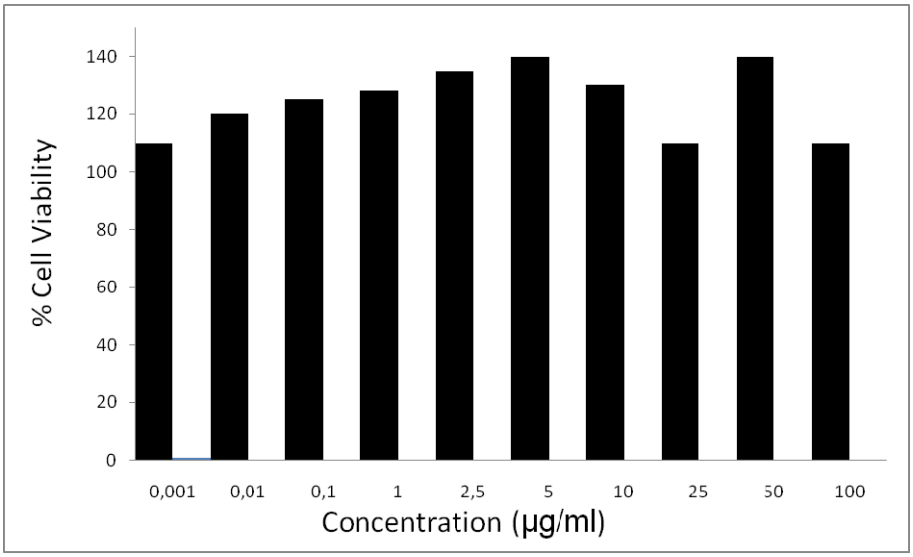

Figure 4.8 MTT results for Thiourea in PC3 cells for 1 day

4.2. Trypan Blue Staining

Trypan blue is a vital stain used to selectively colour dead cells blue. It is a diazo dye. Live cells with intact cell membranes are not coloured, hence, dead cells are shown as a distinctive blue colour under a microscope. Trypan blue staining is a simple way to assume cell proliferation or death.

A549 and BEAS-2B cell lines were kindly provided by Professor Doctor Hasan Bayram (Gaziantep University, Medical School).

During this procedure, 100 µL volume of MCF7, A549 and Beas2B cell suspensions, which were incubated for 24 hours with synthesized A9 and A10 nanoparticles, were placed in appropriate tubes and 200 µL volume of 0.5% Trypan blue was added in each tube and let stand for 2 minutes at room temperature.

The coverslip was placed over the counting chambers of hemocytometer. Both counting chambers were loaded with the cell suspensions using a micropipette. 10 µL would be required per side. The pipette tip was placed at the edge of the coverslip, and the cell suspension was allowed to fill the space by capillary action. The entire volume of the chamber was filled and the number of viable (unstained) cells were counted.

Trypan blue measurements reveal that the A549 and MCF7 cancer cells are not affected by the nanocrystals at any dosage, but lethal effects are determined at the concentration of 50µg/ml for the BEAS-2B cells. The BEAS 2B cells are very sensitive to the nanocrystals and do not proliferate at concentration of 0.5µg/ml.

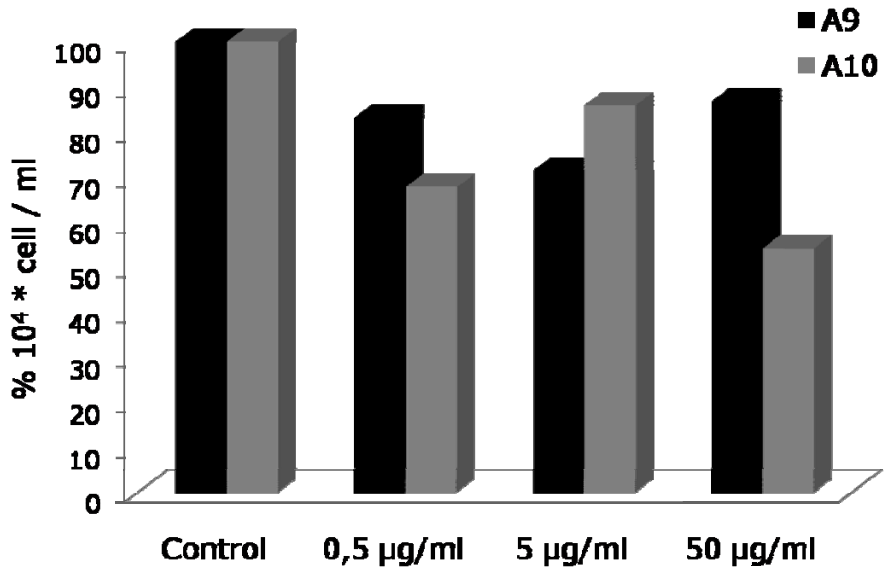

Figure 4.9. % Cell viability of A9 and A10 nanocrystals in A549 cell lines.

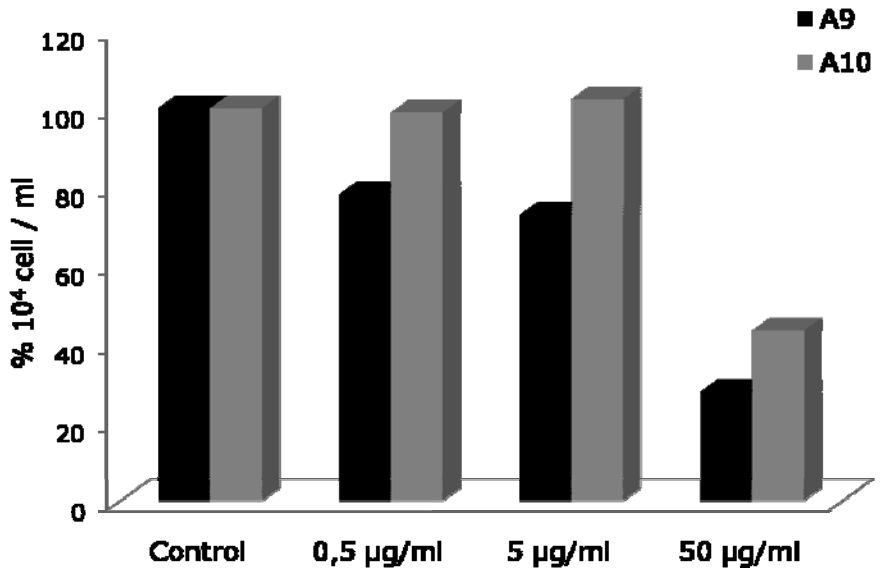

Figure 4.10. % Cell viability of A9 and A10 nanocrystals in BEAS-2B cell lines.

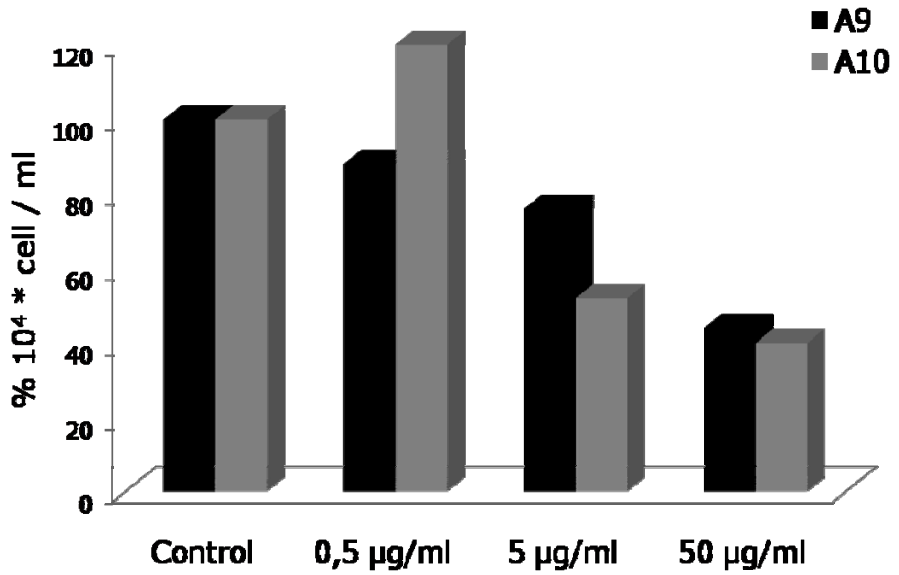

Figure 4.11. % Cell viability of A9 and A10 nanocrystals in MCF7 cell lines.

4.3. Confocal Microscopy

Confocal microscope was used to determine whether the nanoparticles can interact with MCF7 cancer cells or not. Secondly, it was used to verify the location of the CdSeTe/CdS nanoparticles in the PC3 and MCF7 cells.

MCF7 cell line was obtained from Professor Neşe Atabey (Dokuz Eylül University, Medical School, Department of Medical Biotechnology and Genetics).

1.0µg/ml CdSeTe and CdSeTe/CdS nanocrystals in PBS solution were injected in to cell medium in 6-well plates, and then incubated for 1hour at 37^0C. The media was aspirated from wells and washed with PBS, then cells was fixed with paraformaldehyde for 10 minute and fixative solution aspirated and wash with PBS for 5-10 minutes by shaking. The cells were blocked with 10% FBS in PBS for 30 minutes with vigorous shaking and washed with PBS three times and slides were removed from wells and dried. The mounting media was droped onto slide and cover the dried coverslip, then slides were analysed under confocal microscope with 488 nm laser.

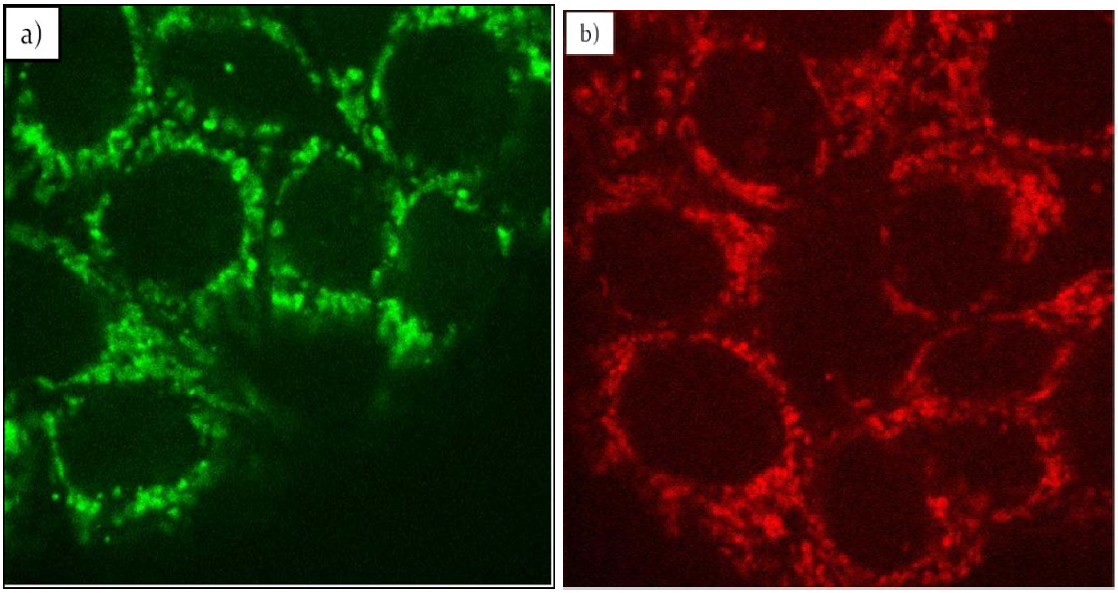

Figure 4.12. Confocal microscopy images of a) A11 - $CdSe_xTe_{1-x}$ (λ_{em}=545nm) and b) A9 - $CdSe_xTe_{1-x}$/CdS (λ_{em}=600nm), (λ_{laser}=488nm).

CdSeTe core nanoparticles have fluorescence emission at 545nm, which gives green light under UV light (Figure 4.12 - a) and CdSeTe/CdS core/shell nanoparticles have fluorescence emission at 600nm where the particles give orange color under UV light (Figure 4.12 - b). In confocal microscopy images in Figure 4.12 (a) and (b), it is seen that both CdSeTe/CdS and CdSeTe nanoparticles penetrate into MCF7 cells and disperse in cell cytoplasm, however they do not enter the nucleus of cells.

We investigated the effect of incubation period on cells exposed to nanoparticles. Different incubation periods and different concentrations of A9-CdSeTe/CdS core/shell and A11-CdSeTe core nanoparticles were used with MCF7 cell lines in confocal imaging applications.

In Figure 4.13 the images of MCF7 cells, which contain 0.05µg/ml A9-nanoparticles, can be seen. In Figure 4.13 (a) and (b) bright field and confocal images after 10min incubation period and in (c) and (d) bright field and confocal images after 30min incubation period are shown, respectively. The nanoparticles were penetrated into MCF7 cells and dispersed in cell cytoplasm, for both 10min and 30min.

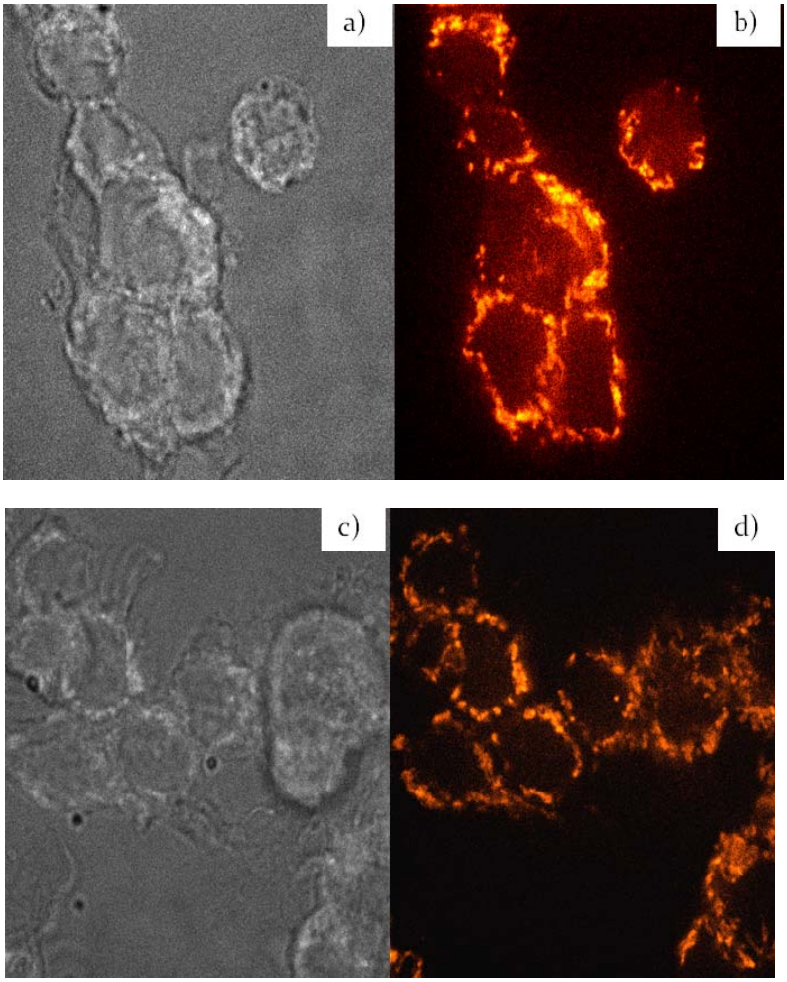

Figure 4.13. Confocal microscopy images of A9 – CdSeTe/CdS with 0,05µg/ml concentration (λ_{em}=600nm). a) bright field image after 10min incubation b) colored confocal image after 10 min incubation c) bright field image after 30min incubation d) colored confocal image after 30 min incubation time, (λ_{laser}=488nm).

In Figure 4.14 the images of MCF7 cells which contain 0.1µg/ml A9-nanoparticles were taken. In Figure 4.14 confocal image of MCF7 cells can be seen after (a) 5min, (b) 10min, (c) 30min. The larger amounts of nanoparticles were penetrated into MCF7 cells after 30min incubation period than both 5min and 10min incubation periods. Both 5min and 10min incubation periods were enough for penetration into cell, but as the incubation period increases, the amount of nanoparticles in cell cytoplasm and aggregation were increased.

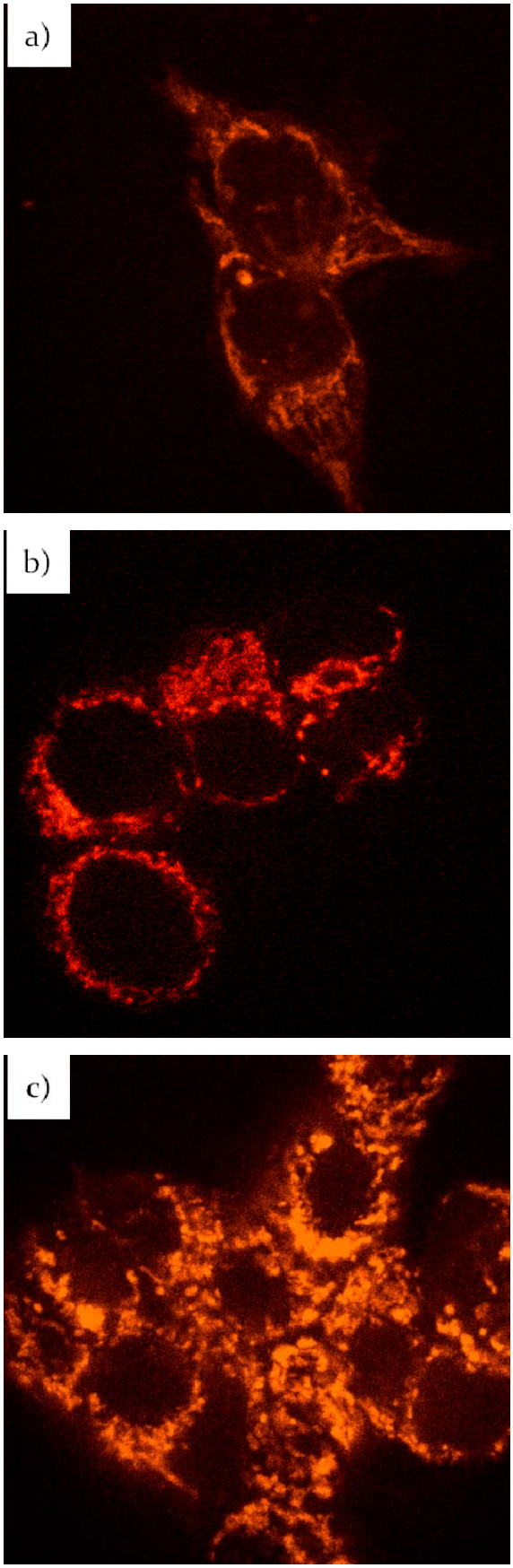

Figure 4.14. Confocal microscopy images of A9 – CdSeTe/CdS (λ_{em}=600nm) with 0.1µg/ml concentration. a) 5min b) 10min c) 30min incubation times, (λ_{laser}=488nm).

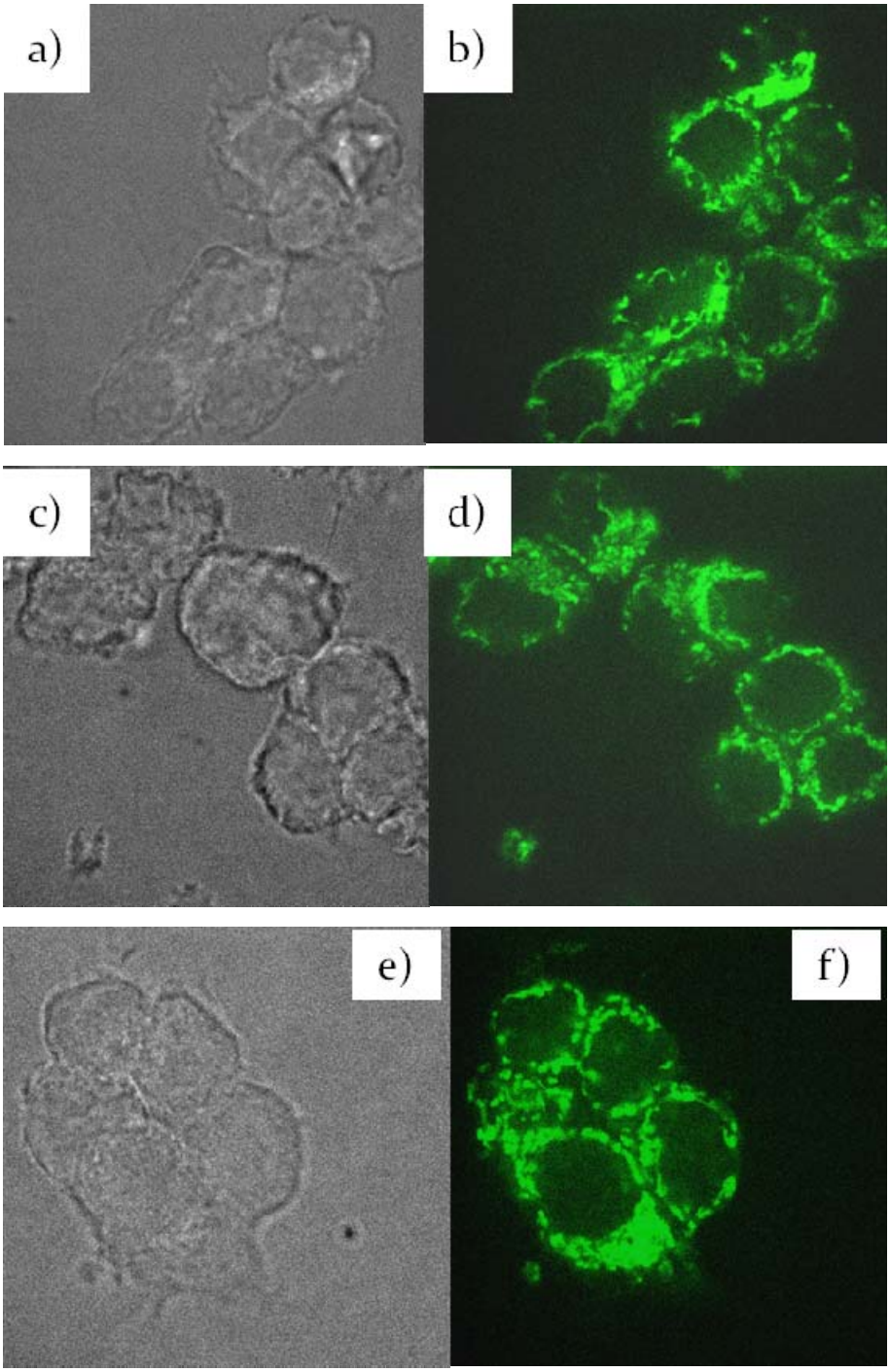

Figure 4.15. Confocal microscopy images of A11 – CdSeTe (λ_{em}=545nm) with 0.05µg/ml concentration. a) bright field image after 5 min incubation b) colored confocal image after 5 min incubation c) bright field image after 10 min incubation d) colored confocal image after 10 min e)bright field image after 30 min incubation f) colored confocal image after 30 min incubation time, (λ_{laser}=488nm).

In Figure 4.15 both confocal and bright field images of A11 – CdSeTe with .05µg/ml concentration can be seen. These three incubation periods were enough for

penetration into cell cytoplasm. After 30 min incubation period (Figure 4.15 (f)) some aggregate formation was observed.

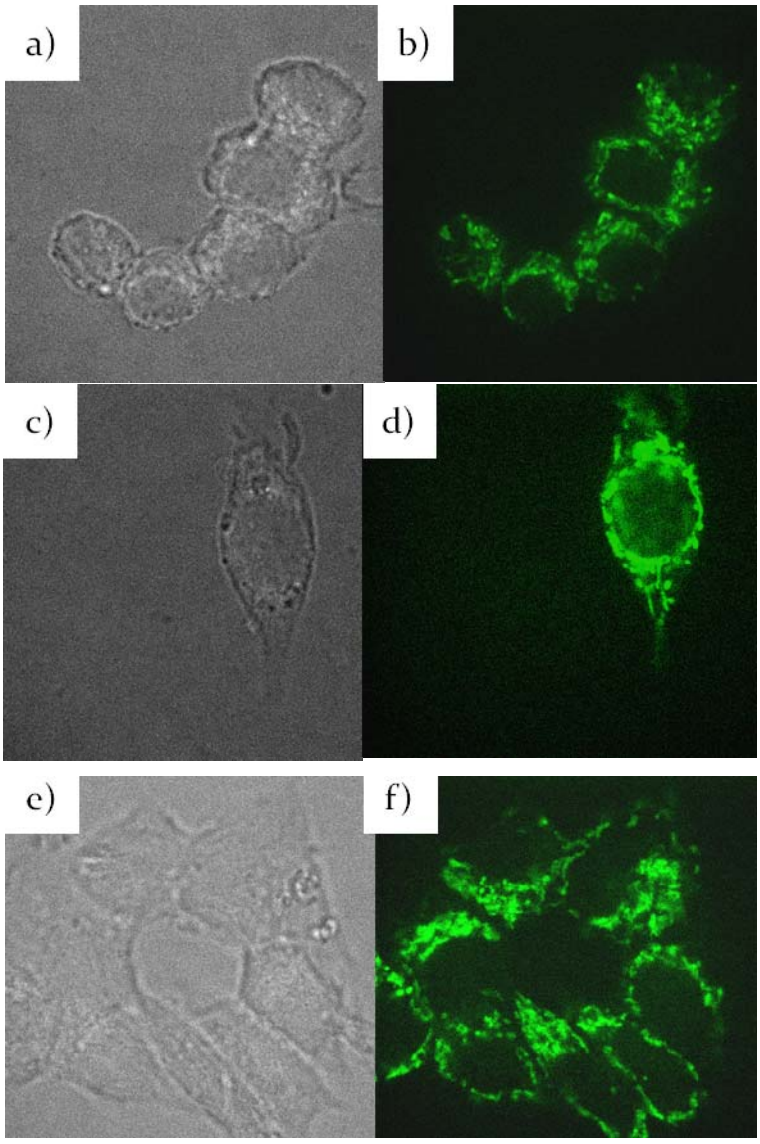

Figure 4.16. Confocal microscopy images of A11–CdSeTe (λ_{em}=545nm) with 0.1µg/ml concentration. a) bright field image after 5 min incubation b) colored confocal image after 5 min incubation c) bright field image after 10min incubation d) colored confocal image after 10 min e)bright field image after 30 min incubation f) colored confocal image after 30 min incubation time, (λ_{laser}=488nm).

In Figure 4.16 confocal and bright field images of A11–CdSeTe with 0.1µg/ml concentration can be seen. Figure 4.15 shows (a) bright field image after 5min incubation, (b) shows colored confocal image after 5min incubation, (c) shows bright field image after 10min incubation, (d) shows colored confocal image after 10min, (e) shows bright field image after 30min incubation, (f) shows colored confocal image after

30 min incubation time. For 0.1μg/ml A11 – CdSeTe nanoparticles, the amount of nanoparticles that penetrated into cell cytoplasm were increased as the incubation time increased.

CHAPTER 5

CONCLUSION

Water dispersible, TGA capped alloy $CdSe_xTe_{1-x}$ core and $CdSe_xTe_{1-x}$ / CdS core/shell nanocrystals were synthesized by a single step aqueous synthesize method below 100^0C. After optimization of the suitable mole ratios of reactants and reaction conditions, characterization was performed by using spectroscopic methods, XRD, TEM and confocal microscopy.

Optimum reaction conditions and molar ratios were determined based on the photoluminesence quantum yield obtained from nanocrystals. Upon testing different TGA/Cd ratios from 4.8 to 1.6 it was conclude that decreasing mole ratio of the TGA/Cd leads to a increase in the photoluminesence quantum yield of the particles. Also, different Se/Te ratios from 0.1:0.9 to 0.5:0.5 were tested. Se/Te mole ratio have also an important role, as the mole ratio of Se is decreased in reaction the photoluminesence quantum yield of the particles is increased.

Spectral properties of nanocrystals can be tuned by size controlling reflux time. Size dependent spectral properties were monitored by fluorescence and UV-Vis spectra. Fluorescence quantum yields scale up to 22% with 50nm FWHM. The size of CdSeTe/CdS nanoparticles varies from 3.7 nm to 5 nm.

The high quantum yields and narrow spectral widths indicates that, the alloy nanocrystals are highly crystalline in structure and monodisperse in size.

Optimized synthesis provides TGA-capped CdSeTe/CdS nanocrystals with bright (22% quantum), emission tunable from 534 to 610 nm. They can be excited from 350nm to 600nm. The energy band gap of the synthesized nanocrystals was estimated by the absorption measurements. As the particle size increases the energy gap of nanoparticles decreases from 2.15 eV to 1.88 eV.

According to the literature, crystal structure of synthesized CdSeTe/CdS nanoparticles is estimated to have, zinc blend form. CdS shell formation around CdSeTe

alloy can be estimated from XRD pattern. After the CdS shell formation, XRD peaks shift to higher diffraction angles, close to 2□ degree of the bulk CdS.

Average crystalline sizes of CdSeTe/CdS nanoparticles were determined by using Debye – Scherrer equation (Equation (1.4)). Particle size of core/shell CdSeTe/CdS nanoparticles were determined from 1.7 nm, to 3.2nm, sampled at different reaction times.

MTT tests were proved that toxicity of CdSeTe/CdS nanoparticles below 1.0μg/ml concentration are not lethal for PC3 and MCF7 cells and this concentration is suitable for biological applications and confocal microscopy studies. Lethal concentrations of $CdCl_2$ and thiourea were also determined by MTT test. Lethal concentration of Cd^{2+} ions was 15.0μg/ml for MC7 cells and 2.5μg/ml for PC3 cells. Thiourea is not toxic for MCF7 and PC3 cells.

Trypan blue measurements reveal that the A549 and MCF7 cancer cells are not affected by the nanocrystals but he BEAS-2B cells are very sensitive to the nanocrystals and do not proliferate at concentration of 0.5μg/ml.

Confocal microscope was used to monitor the nanoparticles in MCF7 cancer cells. Microscopy images show that, after one hour incubation time, alloy CdSeTe core (λem=545nm) and CdSeTe/CdS core/shell nanoparticles (λem=600nm) were successfully enter and stay in cell cytoplasm. Both core and core/shell nanoparticles are suitable for cell imaging applications.

REFERENCES

Åkerman, Warren C. W. Chan, Pirjo Laakkonen, Sangeeta N. Bhatia, and Erkki Ruoslahti 2002. "Nanocrystal targeting in vivo" *Proceedings of the National Academy of Sciences* 99: 20 12619

Alivisatos Paul, 2004. "The Use of Nanocrystals in Biological Detection" *Nature Biotechnology, 22*

Alivisatos, Marcel Bruchez Jr., Mario Moronne, Peter Gin, Shimon Weiss 1998. "Semiconductor Nanocrystals as Fluorescent Biological Labels" *Science* 281: 2013

Bailey and Shuming Nie2003. "Alloyed Semiconductor Quantum Dots: Tuning the Optical Properties without Changing the Particle Size" *Journal of American Chemical Society* 125: 7100-7106

Balet,L.P.; Ivanov,S.A.; Piryatinski,A.; Achermann,M.; Klimov,V.I. 2004. "Inverted Core/Shell Nanocrystals Continuously Tunable between Type-I and Type-II Localization Regimes" *Nano Letters*, 4: 1485-1488

Bhatia, Austin Derfus, Warren C. Chan 2004. "Intracellular Delivery of Quantum Dots for Live Cell Labeling and Organelle Tracking" *Advanced Materials*, 16:12

Bleuse, Sophie Carayon, Peter Reiss, 2004. "Optical properties of core/multishell CdSe/Zn(S,Se) nanocrystals" *Physica E* ,21: 331 – 335.

Bruchez M, Moronne M, Gin P, Weiss S, Alivisatos AP 1998. "Semiconductor Nanocrystals as Fluorescent Biological Labels". *Science*, 281: 2013-2016

Chan and Shuming Nie 1998. "Quantum Dot Bioconjugates for Ultrasensitive Nonisotopic Detection" *Science* 281, 2016

Deerinck Thomas J. 2008. "The Application of Fluorescent Quantum Dots to Confocal, Multiphoton, and Electron Microscopic Imaging" *Toxicologic Pathology*,36

Deka, Alessandra Quarta, Maria Grazia Lupo, Andrea Falqui,Simona Boninelli, Cinzia Giannini,Giovanni Morello, Milena De Giorgi, Guglielmo Lanzani, Corrado Spinella,Roberto Cingolani, Teresa Pellegrinoand Liberato Manna 2008. "CdSe/CdS/ZnS Double Shell Nanorods with High Photoluminescence

Efficiency and Their Exploitation As Biolabeling Probes" *Journal of American Chemical Society* 131:2948-2958

Deng, D. W.; Y, J. S.; Pan, Y. 2006. "Water-Soluble CdSe and CdSe/CdS Nanocrystals: A Greener Synthetic Route". *Journal of Colloid and Interface Science* , 299: 225-232.

Deng, Jun-Sheng Yu , Yi Pan 2006. "Water-soluble CdSe and CdSe/CdS nanocrystals: A greener synthetic route" *Journal of Colloid and Interface Science*, 299 :225–232

Edwards, Steven. 2006. *The Nanotech Pioneers: Where Are They Taking Us?*. Weinheim. England: WILEY-VCH Verlag gmbh & Co.

Fabien Pinaud, Shara C. Williams, Wolfgang J. Parak, Daniela Zanchet,Shimon Weiss,and A. Paul Alivisatos 2001. "Synthesis and Properties of Biocompatible Water-Soluble Silica Coated CdSe/ZnS Semiconductor Quantum Dots" *Journal of Physical Chemical B 105:* 8861-8871

Gaponik, N.; Talapin, D. V.; Rogach, A. L.; Hoppe, K.; Shevchenko, E. V.Kornowski, A.; Eychmuller, A.; Weller, H. 2002. "Thiol-Capping of CdTe Nanocrystals: An Alternative to Organometallic Synthetic Routes." *Journal of Physical Chemistry* B, 106: 7177-7185.

Gu, Lei Zou, Zheng Fang,Weihong Zhu, Xinhua Zhong. 2008. "One-pot synthesis of highly luminescent CdTe/CdS core/shell nanocrystals in aqueous phase" *Nanotechnology* 19:135604

Ibáñez-Peral, Peter L. Bergquist , Malcolm R. Walter, Moreland Gibbs, Ewa M. Goldys 2008."Potential Use of Quantum Dots in Flow Cytometry" *International Journal of Molecular Sciences*,ISSN 1422-0067

J. Geens, K. Peeters, B. Van der Bruggen and C. Vandecasteele 2005. "Polymeric nanofiltration of binary water–alcohol mixtures: Influence of feed composition and membrane properties on permeability and rejection " *Journal of Membrane Science, 255: 255-264*

Kagan, C. B. Murray, M. Nirmal, and M. G. Bawendi 1996. "Electronic Energy Transfer in CdSe Quantum Dot Solids" *Physical Rewiew Letters*,

Kumar and Thomas Nann 2006. "Shape Control of II–VI Semiconductor Nanomaterials" *Small*, 2: 316 – 329

Kumar , V. N. Singh, B. R. Mehta , Gurmeet Singh, S. M. Shivaprasad , Rita Kakkar 2008. "Formation of water-soluble and biocompatible TOPO-capped CdSe

quantum dots with efficient photoluminescence" *Journal of Materials Science*,10856:3494

Manna L, Scher EC, Alivisatos PA. 2000. "Synthesis of soluble and processable rod-, arrow-, teardrop-, and tetrapodshaped CdSe nanocrystals". *Journal of American Chemical Society*. 122:12700–6

Murray and C. R. Kagan and M. G. Bawendi. 2000. Synthesis and characterization of monodisperse nanocrystals and close packed nanocrystal assemblies *Annual Review of Materials Science* 30:545–610.

Murray, C. B.; Norris, D. J.; Bawendi, M. G. 1993. "Synthesis and Characterization of nearly Monodisperse Cde (E = S, Se, Te) Semiconductor Nanocrystallites." *Journal of American Chemical Society* 115: 8706-8715.

Peng X, Manna L, Yang W, Wickham J, Scher E, et al. 2000. "Shape control of CdSe nanocrystals". *Nature* 404:59–61

Peng X,Wickham J, Alivisatos AP. 1998. "Kinetics of II–VI and III–V colloidal semiconductor nanocrystal growth: "focusing" of size distributions." *Journal of American Chemical Society* 120:43–44

Peng X. 2002. "Green chemical approaches toward high-quality semiconductor nanocrystals." *Chemistry European Journal.* 8: 335–339

Peng, Lijuan Zhang, Christian Soeller, Jadranka Travas-Sejdic. 2007. "Preparation of water-soluble CdTe/CdS core/shell quantum dots with enhanced photostability" *Journal of Luminescence* 127:721–726.

Pinaud, Xavier Michalet, Laurent A. Bentolila, James M. Tsay, Soren Doose, Jack J. Li, Gopal Iyer and Shimon Weiss 2005. "Advances in fluorescence imaging with quantum dot bio-probes" *Biomaterials*, 27: 1679-1687

Piven, Andrei S. Susha, Markus Do#blinger, and Andrey L. Rogach 2008. "Aqueous Synthesis of Alloyed CdSexTe1-x Nanocrystals" *Journal of Physical Chemical Society* 112: 15253–15259

Qu, Lianhua, Z. Adam Peng, and Xiaogang Peng 2001. "Alternative Routes toward High Quality CdSe Nanocrystals." *Nano Letters* 1:

Reiss , S. Carayon , J. Bleuse, A. Pron 2003. "Low polydispersity core/shell nanocrystals of CdSe/ZnSe and CdSe/ZnSe/ZnS type: preparation and optical studies" *Synthetic Metals* 139: 649–652

Reiss Peter 2007. “ZnSe based colloidal nanocrystals: synthesis, shape control, core/shell, alloy and doped systems” *New Journal of Chemistry* 31: 1843–1852

Reiss peter, Myriam Protire 2007. “Highly Luminescent Cd1_xZnxSe/ZnS Core/Shell Nanocrystals Emitting in the Blue–Green Spectral Range” *Small* , 3: 399 – 403.

Rogach, A. L.; Kornowski, A.; Gao, M. Y.; Eychmuller, A.; Weller, H. 1999. “Synthesis and Characterization of a Size Series of Extremely Small Thiol-Stabilized CdSe Nanocrystals.” *Journal of Physical Chemistry* B, 103: 3065-3069

Rogach, A. L.; Nagesha, D.; Ostrander, J. W.; Giersig, M.; Kotov, N. A. 2000. "Raisin Bun"-Type Composite Spheres of Silica and Semiconductor Nanocrystals.” *Chemical Materials* 12:2676-2685.

Rogach, Thomas Franzl, Thomas A. Klar, Jochen Feldmann, Nikolai Gaponik, Vladimir Lesnyak, Alexey Shavel, Alexander Eychmu1ller, Yuri P. Rakovich, and John F. Donegan. 2007. **“**Aqueous Synthesis of Thiol-Capped CdTe Nanocrystals: State-of-the-Art.” *Journal Physical Chemistry C* 111: 14628-14637

Sun, Y S Liu, P T Vernier, C H Liang, S Y Chong, Lmarcu and M A Gundersen 2006. “Photostability and pH sensitivity of CdSe/ZnSe/ZnS quantum dots in living cells” *Nanotechnology* 17:4469–4476

Talapin Andrey L. Rogach, Ivo Mekis, Stephan Haubold , Andreas Kornowski, Horst Weller 2002. “Synthesis and surface modification of amino-stabilized CdSe, CdTe and InP nanocrystals” *Colloids and Surfaces A*:, 202: 145–154

Talapin, D. V.; Rogach, A. L.; Kornowski, A.; Haase, M.; Weller, H. Highly 2001. “Luminescent Monodisperse CdSe and CdSe/ZnS Nanocrystals Synthesized in a Hexadecylamine-Trioctylphosphine Oxide-Trioctylphospine Mixture”. *Nano Letters,* 1: 207-211

Talapin, Ivo Mekis, Stephan Gtzinger, Andreas Kornowski, Oliver Benson, and Horst Weller 2004. “CdSe/CdS/ZnS and CdSe/ZnSe/ZnS Core−Shell−Shell Nanocrystals” *Journal of Physical Chemical B* 108: 18826-18831

Talapin, James H. Nelson, Elena V. Shevchenko, Shaul Aloni, Bryce Sadtler, A. Paul Alivisatos 2007. “Seeded Growth of Highly Luminescent CdSe/CdS Nanoheterostructures with Rod and Tetrapod Morphologies” *Nano Letters* , 7: 2951-2959

Wang, Daocheng Pan, Shichun Jiang, Xiangling Ji,Lijia An, and Bingzheng Jiang. 2005. "A New Two-Phase Route to High-Quality CdS Nanocrystals". *Chemistry European Journal* 11: 3843 – 3848.

Wang, Zhiyong Tang, Miguel A. Correa-Duarte, Isabel Pastoriza-Santos,Michael Giersig, Nicholas A. Kotov,Luis M. Liz-Marza´n 2004. "Mechanism of Strong Luminescence Photoactivation of Citrate-Stabilized Water-Soluble Nanoparticles with CdSe Cores" *Journal of Physical Chemical B* 108: 15461-15469

Wen Jiang, Anupam Singhal, Jianing Zheng, Chen Wang, and Warren C. 2006. "Optimizing the Synthesis of Red- to Near-IR-Emitting CdS-Capped CdTe*x*Se1-*x* Alloyed Quantum Dots for Biomedical Imaging". *Chemical Materials* 18: 4845-4854.

Wolcott, Daniele Gerion,Micah Visconte,Jia Sun,Schwartzberg,Shaowei Chen, Jin Z. Zhang 2006. "Silica-Coated CdTe Quantum Dots Functionalized with Thiols for bioconjugation to IgG Proteins" *Journal of Physical Chemical B*, 110

Wu, Hongjian Liu, Kari Haley, Joseph Treadway, Peter Larson, Marcel Bruchez 2002. "Immunofluorescent labeling of cancer marker Her2 and other cellular targets with semiconductor quantum dots" *Nature Biology* 21: 1038

Zhang, Zhen Zhou, Bai Yang, and Mingyuan Gao 2003. "The Influence of Carboxyl Groups on the Photoluminescence of Mercaptocarboxylic Acid-Stabilized CdTe nanoparticles" *Journal of Physical Chemical ,* 107: 8-13